Role of the C-terminal cytoplasmic tail of the NhaP2 antiporter from *Vibrio cholerae* in transmembrane ion transport

by

Evan Jonathan Wiens

A Thesis submitted to the Faculty of Graduate Studies of

The University of Manitoba

in partial fulfillment of the requirements of the degree of

Master of Science

Department of Chemistry

University of Manitoba

Winnipeg, Manitoba, Canada

Abstract

Although the importance of cation/proton antiporters in cellular physiology is well recognized and widely studied, many antiport systems remain underinvestigated. In this work, I report the phenotypic and biochemical effects of deletion of the cytoplasmic C-terminal tail of the NhaP2 antiporter from *Vibrio cholerae* (Vc-NhaP2). Namely, deletion of the C-terminal tail results in diminished K^+/H^+ and Na^+/H^+ antiport activity, as well as a 5-fold decrease in affinity for its major substrate, K^+ (measured as the apparent K_m at pH 7.5). Furthermore, reconstitution of antiport activity in the truncation mutant upon addition of exogenous C-terminal tail is demonstrated. Currently, the only known mechanism of antiport is for NhaA, which lacks a cytoplasmic tail. Therefore, these results suggest that NhaP2 may employ a novel mechanism of antiport in which the cytoplasmic tail is directly or indirectly involved.

Acknowledgements

Many thanks are due to Dr. Jörg Stetefeld and Dr. Pavel Dibrov for their guidance, support, and trust.

Special thanks are due to Dr. Judith Winogrodzki and Dr. George Orriss for their guidance, assistance, and willingness to share with me their wealth of knowledge.

Thanks to Dr. Sean McKenna and Dr. Mazdak Khajehpour for their critical reading and helpful analysis of this work.

Financial support from the Faculty of Graduate Studies, Faculty of Science, and Department of Chemistry is also acknowledged and appreciated.

Table of Contents

page #

List of Figures

1. Introduction

1.1 ROLES OF CATION/H^+ ANTIPORTERS IN PROKARYOTIC CELLULAR PHYSIOLOGY

Cation/proton antiporters are ubiquitous in all forms of life and play a variety of vital functions in the cell. Roles established to date include maintaining intracellular pH and intracellular cation homeostasis, the regulation of cell volume (primarily, Na^+ and K^+ exchange for H^+)[1], and also contributing to the establishment of the Na^+ gradient across the plasma membrane that is of great importance in the energetics of bacteria, including many pathogens such as *Vibrio cholerae*[2]. In many organisms, this Na^+ gradient is important for ATP synthesis, symport of certain metabolites (such as glucose and a number of amino acids), and also as an energy source that drives the rotation of the bacterial flagellum[3]. Furthermore, establishment of this gradient seems to be involved in establishment of pathogenesis in *Vibrio cholerae*[4]. As such, it is important that we characterize the proteins which contribute to the establishment and maintenance of these gradients.

1.1.1 MAINTENANCE OF CELLULAR CATION CONCENTRATION, pH, AND VOLUME.

A main function of cation/H^+ antiporters in prokaryotes is to maintain intracellular cation concentrations. Under normal circumstances, if ionic equilibrium of cations such as Na^+ and K^+ was allowed to be established, it would result in toxic levels

of cations inside the cell. Therefore, it is necessary for the bacterium to possess mechanisms to extrude these cations. The major mechanism by which this is achieved is to use the H^+ gradient generated by the electron transport chains and/or ATPases as an energy source for facilitated transport of cations out of the cell. The secondary transporters involved in this process are antiporters and, as such, they are crucial for bacterial survival in media of even modest ionic strength.

However, when challenged in a low-pH environment, antiporters can facilitate the extrusion of H^+ from the cytoplasm in exchange for cations. Such a situation occurs, for example, in the NhaP1 antiporter from the archaea *Methanococcus,* which exhibits maximal antiport activity around pH 6.0[5]. In this way, the bacterium is able to resist cytoplasmic pH equilibration with the low-pH medium, and hence is able to survive.

Antiporters are also important in the regulation of cell volume in bacteria. Cell volume is primarily determined by the amount of water present in the cell; the amount of water present in the cell is in turn dependent on the concentration of osmolytes within the cell. Therefore, a cell can regulate its volume by preferentially allowing transport of cations either into or out of the cell, depending upon whether a small or larger volume is required. Antiporters play an important role in mediating such transport[6].

1.1.2. MAINTENANCE OF Na^+-MOTIVE FORCE

Many bacteria generate a Na^+-motive force as a vital endpoint of cellular metabolism, both for the generation of ATP and for other processes, such as symport of primary metabolites and as an energy source for rotation of the bacterial flagellum[7].

The Na^+-translocating NADH:quinone oxidoreductase (NQR) is a functional analogue (although not a homolog) of Complex I of the classical electron transport chain[8]. It facilitates the translocation of Na^+ across the membrane upon oxidation of the NADH generated as a result of catabolic pathways such as the tricarboxylic acid cycle. This Na^+ gradient can then be used for the generation of ATP in the same way that the H^+ gradient is used in the classical electron transport chain. Specifically, Na^+ ions fall down their concentration gradient through a Na^+-dependent ATPase of the classical F_1F_0-type; the resulting rotation of the enzyme catalyzes the formation of ATP from ADP and inorganic phosphate[9]. In some species, this is the primary means of ATP generation.

Many substrates depend on the presence of a sodium gradient for entrance into the cell. For example, it has been shown that in *Staphylococcus aureus,* uptake of the sulfonated amino acid taurine is dependent on the presence of external sodium[10]. Also, it has been shown that the sodium gradient plays an important role in glucose uptake in many bacterial species, including *Vibrio parahaemolyticus*[11]. In addition, experiments have shown that amino acid transport in many bacteria is heavily dependent on Na^+ symport[12].

In many bacterial species, including members of the genus *Vibrio*, flagellar rotation, and hence motility and chemotaxis are dependent fully on the translocation of Na^+ ions down their concentration gradient. The translocation of these ions provides the necessary energy for flagellar rotation; specifically, the influx of Na^+ down its concentration gradient induces movement in the flagellar stator complex which, by means of its physical association with the rotor complex, induces rotation[13].

Antiporters play a central role in regulating this gradient. For example, the Na^+ gradient can be generated by influx of H^+ down its concentration gradient as facilitated by an antiporter; conversely, the Na^+ gradient can be dissipated by the same mechanism in order to generate an H^+ gradient if needed. Therefore, Na^+/H^+ antiporters are links between transmembrane H^+ and Na^+ circulation, and as such are necessary for any cells which require the establishment and maintenance of a Na^+ gradient.

1.1.3. ROLE OF Na^+ GRADIENT IN PATHOGENESIS

The establishment of a Na^+ gradient has been shown to be crucial in the pathogenesis associated with many bacterial agents, including *V. cholerae*[14] and *Yersinia enterocolitica*[15]. Since initial colonization and even toxin export are dependent on the functional presence of flagella, which are in turn dependent in many species on the presence of the Na^+ gradient, establishment and maintenance of the Na^+ gradient are crucial steps in the pathogenic cycle of these bacteria. Furthermore, the important human pathogens *Treponema pallidum, Chlamydia trachomatis,* and *C. pneumoniae* appear to utilize an Na^+-dependent F_1F_0-ATPase as their only means of ATP synthesis[16].

In *V. cholerae,* maintenance of the Na^+ gradient seems to be directly related not only to adhesion and motility, but to the expression of virulence factors; dissipation of the Na^+- motive force using ionophores, mutations to *nqr,* and inhibition of NQR proved to modulate the expression of virulence-related genes[17,18]. Furthermore, changes in the Na^+ cycle in *V. cholerae* resulted in altered expression of the regulatory membrane proteins TcpP and TcpH, which are in turn required for expression of ToxT; ToxT is a

crucial transcriptional activator of the important virulence factors in *V. cholerae* infection, including cholera toxin.

Therefore, the Na^+ gradient is clearly important in the virulence of many important human and animal pathogens and, as discussed previously, antiporters play a central role in the establishment and maintenance of this gradient.

1.2. BIOCHEMICAL AND PHYSIOLOGICAL PROPERTIES OF Vc-NhaP2

Although Peter Mitchell postulated the presence of K^+/H^+ antiporters half a century ago, the existence of this seemingly important class of transmembrane ion transporters has only recently been proven[19]. Though a number of protein systems responsible for transmembrane K^+ exchange have been identified and studied, these systems are only active under conditions of extreme stress, such as when the cell is in a hypoosmotic environment or when intracellular K^+ levels rise dangerously high[20]. Interestingly, however, the antiporters responsible for maintaining K^+ levels in normal circumstances, in the same way that antiporters such as NhaA maintain Na^+ levels, remained undiscovered. However, a candidate for such a "housekeeping" K^+/H^+ antiporter was identified in 2010[21]. Previously annotated as a Na^+/H^+ antiporter, NhaP2 from *Vibrio cholerae* (Vc-NhaP2) was shown to preferentially transport K^+ when in solution along with Na^+; it also transports K^+ with much greater efficiency. The essential role played by Vc-NhaP2 was made evident by deletion studies, which showed that deletion of *Vc-nhaP2* was lethal in *V. cholerae* when grown in media containing high concentrations of K^+ at pH close to 6.0[22].

1.2.1. PROFILE OF ACTIVITY OF Vc-NhaP2

One can make a number of important observations based upon the pH profile of Vc-NhaP2 (Figure 1)[23]. First, it is clear that Vc-NhaP2 transports K^+ with the greatest efficiency of any cation, especially at cytoplasmic pH (pH_{in}) close to normal physiological levels. Second, it is clear that maximal antiport efficiency occurs at normal physiological pH_{in}. These two observations lend themselves clearly to the hypothesis that K^+ is the *in situ* preferred substrate for Vc-NhaP2. Furthermore, its inability to facilitate Li^+/H^+ is a trait unique to certain NhaP-type antiporters, and could prove to make Vc-NhaP2 an important model system for studying molecular mechanisms methods of cation selectivity in secondary transporters. This hypothesis, termed “ligand shading”, will be explicated in further sections.

1.2.2. SUBSTRATE SPECIFICITY OF Vc-NhaP2

Growth experiments using a mutant strain of *V. cholerae* in which Vc-NhaP2 is deleted reveal a lethal phenotype in the presence of high concentrations of potassium in a slightly acidic medium (pH 6.0)[24]. Taken together with the relative efficiency of K^+ transport shown in Figure 1, this finding shows that Vc-NhaP2 functions *in vivo* as a K^+/H^+ antiporter.

In keeping with the hypothesis that K^+ is the *in situ* preferred substrate for Vc-NhaP2, Resch et al. (2010) conducted competition assays to determine its substrate specificity. The addition of Li^+ and Na^+ to the experimental medium increased the K_m for K^+ modestly (from 1.62 mM to 5.95 mM in the case of Na^+, and to 9.00 mM in the case

Figure 1. pH profile of Vc-NhaP2 activity, determined in inside-out sub-bacterial membrane vesicles produced from *E. coli* antiporterless strain TO114 overexpressing Vc-NhaP2. Antiport activity was measured by percent dequenching of lactate-induced acridine orange fluorescence quenching upon addition of LiCl (▲), NaCl (●), and KCl (■). Adapted from Resch et al. (2010)[13].

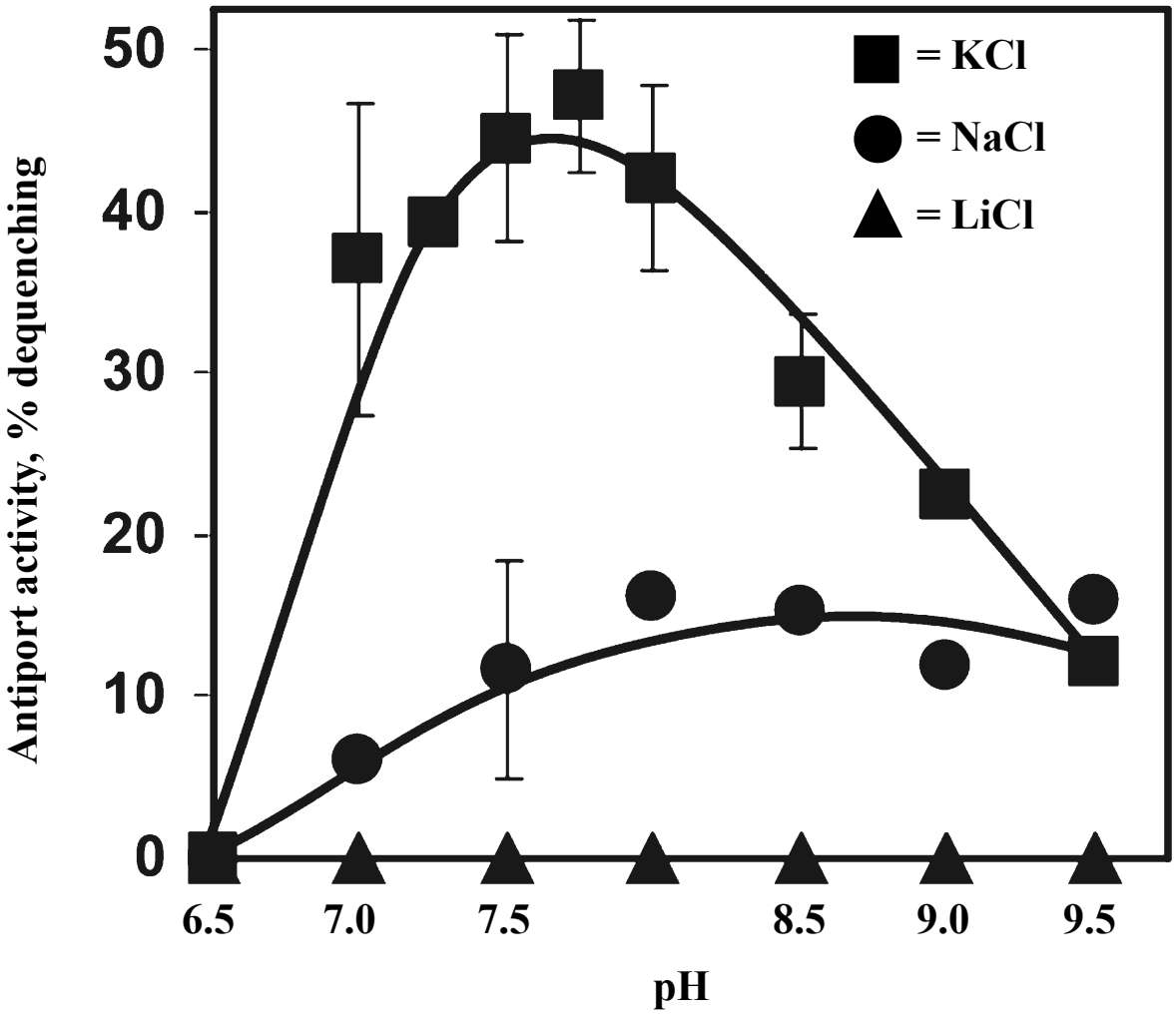

of Li^+). Conversely, addition of K^+ essentially abolished Na^+ antiport. Therefore, it is clear that these cations do still compete with K^+ for access to the binding site, despite the inefficiency (for Na^+) or nonexistence (for Li^+) of antiport for these cations, as shown in Figure 1. Furthermore, Resch et al. also showed that insignificant differences in apparent K_m determined for K^+ (1.62 mM) and for Na^+ (1.04 mM) cannot explain the disparity in antiport efficiency observed in Figure 1. In addition, the above findings show that Li^+ clearly competes for access to the active site, despite Li^+/H^+ transport never occurring.

Therefore, since it is clear that the role of Vc-NhaP2 *in vivo* is to facilitate K^+/H^+ exchange, and since a model based on substrate affinity is insufficient to explain this behavior, a new model is needed. Such a model is proposed by Resch et al. and is termed "ligand-shading".

1.2.3. THE "LIGAND-SHADING" HYPOTHESIS

Antiporters and transmembrane ion channels are able to select cationic substrates with some specificity based on certain physical parameters of the translocated cation. One of the most important of these characteristics is size. Specifically, when competition exists between two cations of differing ionic radii, the size of the active site can be such that the smaller cation is allowed access, while the larger is not. Many Na^+ transporters[25,26,27] use this to select Na^+ over K^+; their active site is large enough to fit Na^+ (1.02 Å) without steric hindrance, but not K^+ (1.38 Å). This mode of selection is commonly referred to as the "size-exclusion principle", and is well known to be important in the functioning of many transmembrane ion transporters.

The size-exclusion principle readily explains the substrate specificity of Na^+/H^+ antiporters such as NhaA, which does not transport K^+ in any situation[28]. However, the mode by which an antiporter might select a larger cation (such as K^+) in preference to a smaller cation (such as Na^+) is unknown. Given that, as described above, Vc-NhaP2 exhibits this K^+-favoring substrate specificity, it becomes an ideal model system for studying substrate specificity in transmembrane ion transporters which exhibit specificity contrary to what would be expected for systems governed by the size-exclusion model.

In order to explain this phenomenon, Resch et al. (2011) proposed the "ligand-shading" hypothesis. Briefly, although all substrate cations (K^+, Na^+, Li^+, H^+) would share the same cation-binding site, the amino acid ligands to which they coordinate may differ. A proton requires only one electronegative ligand in binding to the active site, while alkali cations require at least 6 (up to 8) ligands for binding to a polypeptide[29]. If the binding of Li^+ to the active site (which competition assays indicate does occur) causes the H^+ to be occluded from ("shaded") or knocked off its ligand, Li^+/H^+ exchange would be rendered impossible, since H^+ would never be able to displace a more tightly bound Li^+ ion from its coordination sphere (but Li^+ can easily displace H^+, which has just a single coordination bond).

If the coordination of large substrate cations (such as Na^+ and K^+) does not involve the H^+ binding ligand, antiport could be facilitated. Furthermore, since Li^+ and H^+ apparently share ligands which are not shared with Na^+ or K^+, this permits the Li^+/K^+ and Li^+/Na^+ exchange that indeed has been observed.

Finally, and perhaps most intriguingly, the ligand shading hypothesis can explain why K^+ transport is preferred to Na^+ transport *in situ*, despite the similar K_m of the antiporter for the two cations. If the binding of Na^+ partially shades the H^+ binding ligand and K^+ binding does not, it will make Na^+/H^+ antiport less efficient, resulting in a clear kinetic advantage for K^+[30].

Therefore, the ligand shading hypothesis, in conjunction with the size-exclusion principle, can explain all manners of ion specificity currently known in transmembrane ion transporters. If confirmed to be true, ligand shading could explain not only the peculiar ion specificities of NhaP-type antiporters, but also specificities of other transmembrane ion channels. Structure determination by X-ray crystallography will confirm whether or not the ligand shading hypothesis is indeed the method by which these ion specificities is achieved.

1.3. THE C-TERMINAL CYTOPLASMIC TAIL OF Vc-NhaP2.

An analysis of the Vc-NhaP2 sequence using Swissmodel (ExPASy) predicts that it is comprised of 13 transmembrane segments which are followed by a 120 amino acid cytoplasmic tail at the C-terminal end of the protein. This tail is predicted to consist of ~ 40% α-helix and ~ 15% β-strand, with the remaining ~ 45% of its structure predicted to be random coil. In addition, the C-terminal tail is predicted to have significant domain architecture; specifically, it is predicted to contain a TrkA-C lobe, which itself is predicted to contain a Rossman fold[31]. If confirmed to be true, this would make Vc-NhaP2 the only known prokaryotic antiporter whose cytoplasmic tail contains any form

of domain architecture. As a result, Vc-NhaP2 could potentially be viewed as an interesting functional analogue to mammalian antiporters, which are known to contain significant domain architecture and to play significant regulatory roles in the cell.

Given the difficulties associated with studying integral membrane proteins, we decided to study in more detail the C-terminal cytoplasmic tail of Vc-NhaP2 to gain fresh insights into its role in NhaP2 antiport activity. To do this, a number of physiological and biochemical experiments were performed, with an ultimate goal being to obtain a high resolution structure of the Vc-NhaP2 tail.

1.3.1. TrkA-C LOBES AND ROSSMAN FOLDS

TrkA domains are not well understood, but are known to be well distributed among eubacterial, archaeal, and eukaryotic species. They have been found in a number of divalent cation/Na^+ symporters, amino acid antiporters[32], and in K^+ channels[33]. It is thought that they are involved in the regulation of such channels in a redox-sensitive manner due to their ability to bind dinucleotides such as NAD via the Rossman fold. These domains are found as modular entities, composed of TrkA-C (C-terminal) and TrkA-N (N-terminal) lobes. These lobes can be present either on the same protein or as separate domains on different proteins[34].

A Rossman fold is a tertiary structure found in a wide range of proteins that are known to bind nucleotide cofactors such as nicotinamide adenine dinucleotide (NAD) or flavin adenine dinucleotide (FAD)[35]. This tertiary structure allows a protein to bind or metabolize NAD and FAD, which are both crucial cofactors in many key biological

processes. For example, FAD is an important cofactor for succinate dehydrogenase (Complex II), a component of the electron transport chain, where it is reduced from FAD to $FADH_2$ upon oxidation of succinate[36]. In addition, FAD has been shown to be a cofactor in other oxidoreductases and nitric oxide reductases, including certain cytochrome oxidoreductases, such as the NADPH-cytochrome P450 oxidoreductase (CYPOR). Interestingly, in this protein, the FAD domain undergoes significant conformational changes during the redox interconversion between the bound FAD/ $FADH_2$ forms[37]. In these enzymes, FAD is attached covalently as a cofactor to the FAD domains.

NAD is a crucial metabolite for such basic processes as the Krebs cycle; indeed, the accumulation of reduced NAD is the primary source of energy for generation of the H^+ gradient that is necessary for aerobic production of ATP[38]. This role of NAD as an "electron carrier" stems from its ability to exist in the oxidized (NAD^+) and reduced (NADH) forms. The energetic reduced form is able to reduce (and be oxidized by) prosthetic groups of electron transport chain enzymes (such as the flavin mononucleotide of Complex I), thus facilitating generation of the H^+ gradient.

Similar to NADH, FAD is an important and ubiquitous redox component of diverse electron transport chains. Again, this is due to its ability to exist in a number of relatively stable redox forms: the oxidized (FAD), partially reduced ($FADH\cdot$ "semiquinone"), and fully reduced ($FADH_2$) states. This makes FAD a more versatile electron acceptor/carrier than the nicotinamide adenine dinucleotide redox pair (NAD^+/

NADH) and allows flavoproteins to participate in a wider range of reactions than the NAD(P)-linked dehydrogenases[39].

The oxidation state of nucleotides such as NAD and FAD is directly related to the metabolic state of the cell. Metabolically stressed cells will have a greater FAD:$FADH_2$/ NAD:NADH ratio, whereas cells in which the electron transport chain is well-supplied will have a smaller FAD:$FADH_2$/NAD:NADH ratio. Therefore, FAD or NAD could, in principle, be a sort of "redox sensor" that, depending on its oxidation state, reflects the metabolic status of the cell. Given the integral role antiporters play in modulating the gradients originally generated by the electron transport chain, regulation based on cellular metabolic state (via dinucleotide binding to the Rossman fold) could make Vc-NhaP2 an important regulatory element.

1.4. COMPARISON OF SOLUBLE DOMAINS IN PROKARYOTIC AND EUKARYOTIC CATION/H^+ ANTIPORTERS

There is a wide variation in substrate specificity, fine structure, and cellular function between cation/H^+ antiporters both within and between phyla and kingdoms. While these differences are without a doubt pertinent when examining the subtle differences between antiport systems, only the most fundamental similarities and differences will be considered here.

While prokaryotic antiporters differ vastly from their mammalian counterparts, they do share some basic common features. First, they all consist of multiple transmembrane helices (generally 12) that form a funnel through which the substrates are

exchanged. Second, if a sequence alignment is performed, a pattern of conserved residues can be identified which is consistent between prokaryotic and eukaryotic antiporters, suggesting the possibility of a common antiport mechanism[40].

Despite these similarities, a number of fundamental differences between antiporters of the two different kingdoms exist. First, one of the main functions of prokaryotic antiporters is the extrusion of toxic cations, which is achieved by pumping H^+ in and Na^+ out. However, eukaryotic antiporters generally have the opposite function; they prevent excessive acidification of the cytoplasm (as a result of active glycolysis and other acidifying pathways), and so an intracellular pH of ~ 7.2 is maintained by the import of Na^+ coupled to the extrusion of H^+[41].

Perhaps the most relevant difference, at least for this work, between prokaryotic and eukaryotic antiporters is the structure of the C-terminal cytoplasmic tails of eukaryotic antiporters. First, the C-terminal tails of eukaryotic antiporters tend to be much larger than the tails found in prokaryotic antiporters. Also, eukaryotic antiporters are known to have rich domain architecture that allows them to be regulated and to also interact with and regulate other proteins. For example, the human NHE1 Na^+/H^+ antiporter has a C-terminal tail consisting of 315 amino acids[42], much larger than the predicted 120 amino acids tail of Vc-NhaP2. Furthermore, NHE1 is known to have two regulatory Ca^{2+}-dependent calmodulin binding domains, as well as regions for binding calcineurin homologous protein (CHP) and tescalcin[43]. While the nature of these particular proteins is not important here, the key point is the presence of structured domains.

In contrast, of the over 200 prokaryotic genes that have been annotated as cation/ H^+ antiporters which are predicted to have a C-terminal cytoplasmic tail, none of these predictions show any domain architecture whatsoever, except for Vc-NhaP2[44].

Therefore, if the domain architecture of Vc-NhaP2 could be confirmed by crystallographic structure determination, it would make it the only known prokaryotic antiporter to contain any domain architecture in its C-terminal tail. Furthermore, it would make Vc-NhaP2 an interesting functional analogue to eukaryotic antiporters.

On a functional basis, it is known that deletion of the NHE1 C-terminal tail affects the pH profile of activity of the antiporter[45]. A similar effect has also been seen in prokaryotic examples, such as NhaP1 from *Synechocystis* PCC6803 (SynNhaP1)[46]. Thus, the pH dependence of antiporter function is clearly not dependent upon a structured C-terminal tail, as the tail of SynNhaP1 is unstructured. This hints that the domain architecture predicted for Vc-NhaP2 is involved in processes other than pH dependence.

1.5. EPIDEMIOLOGY OF *V. CHOLERAE*

V. cholerae is a major human pathogen which is estimated to affect between 3-5 million people worldwide per year; it was responsible for ~ 130,000 deaths in 2010[47]. Cholera outbreaks are found almost exclusively in the developing world, where water treatment processes are insufficient and drinking water is often fecally contaminated. It is of special concern following natural disasters such as earthquakes and hurricanes, where demand for water is especially high and the infrastructure cannot meet demand.

While the mortality rate of properly treated *V. cholerae* infection is very low (approximately 1%), when untreated mortality rates can increase to 50-60%[48]. This underscores the importance for effective and widely available treatments. Such treatments ideally include water and electrolyte replacement, but this is made difficult when outbreaks occur in areas where clean drinking water is not easily accessible. Antibiotics can shorten the course of the infection[49], but this approach is becoming increasingly ineffective due to its emerging resistance towards the available antibiotics[50,51,52]. Therefore, development of novel antibiotics as alternative strategies in tackling *V. cholerae* infection is of great importance.

As discussed above, antiporters play a central role in the life cycle and pathogenesis of *V. cholerae*. Furthermore, Vc-NhaP2 has been shown to be essential for survival in low-pH media containing high K^+ concentrations. Finally, if the predicted domain architecture of the C-terminal tail is confirmed, and Vc-NhaP2 plays a regulatory role in the cell, it could further increase the importance of Vc-NhaP2 in cell survival. These factors make Vc-NhaP2 a potentially valuable target for novel antibiotics, and structure determination of the Vc-NhaP2 C-terminal tail could represent a new milestone in designing drugs to limit *V. cholerae* outbreaks.

1.6. RESEARCH OBJECTIVES AND RELEVANCE

The ultimate end-goal of this work is the high resolution structure determination of the Vc-NhaP2 tail. This work is important in a number of respects. First, the canonical mechanism of cation/H^+ antiport was determined from the crystal structure of NhaA,

which has no cytoplasmic C-terminal tail. If the C-terminal tail can be shown to be involved in antiport, Vc-NhaP2 could represent a novel form of antiport differing from that of NhaA. Thus, understanding the role of the C-terminal tail in Vc-NhaP2 antiport has the potential to significantly broaden our understanding of how transmembrane ion transporters function.

Second, as discussed above, the C-terminal tail of Vc-NhaP2 is predicted to be highly structured and to contain domain architecture. This domain architecture could allow Vc-NhaP2 to play a significant regulatory role in the cell, would make Vc-NhaP2 a precedent-setting prokaryotic antiporter, and provide a new paradigm for prokaryotic antiporter structure and function.

In particular, given the enormous public health importance of *V. cholerae*, the characterization and structure of a protein which has been shown in preliminary experiments to be essential for infectivity has to be considered as a key target for rational drug design trials.

For these reasons, characterization of the Vc-NhaP2 tail and its structure determination could represent great progress in both basic and medical science.

2. Materials and Methods

2.1. PCR CONDITIONS

Platinum PCR Supermix High Fidelity DNA polymerase (Invitrogen) was used to amplify the 1.75 kb fragment corresponding to *Vc-nhaP2*. A hanging adenine was added via incubation of the DNA in the presence of 1 unit of Taq DNA polymerase (Fermentas). "Around-the-horn" cloning and cloning of *Vc-nhaP2* for the overexpression vector was done with Phusion High-fidelity DNA polymerase (New England Biolabs). In all cases, a 5 μL aliquot of the PCR mixture was run on a gel to verify the product size, and the remaining PCR mixture was purified using the QIAquick PCR Purification Kit (Qiagen).

For pVc-NhaP2 cloning, the DNA was introduced into the pBAD-TOPO vector using the manufacturer's protocol (Invitrogen). The ligation mixture was then plated onto LB agar plates containing 100 μg/mL ampicillin overnight at 37°C, and plasmid DNA was isolated using the QIAprep Spin Miniprep kit (Qiagen). The fidelity of the PCR was confirmed by DNA sequencing at the Oregon State University Center for Genome Research and Biocomputing core lab facility. The pVc-NhaP2 construct was then introduced into *E. coli* TO114 by chemical transformation.

For pVc-NhaP2Body cloning, the "around-the-horn" PCR involved a 30 second initial denaturing at 98°C, after which the thermocycle program ran as follows: 10 second denaturing at 98°C, 30 second annealing at 65°C, and 3.5 minute extension at 72°C. This cycle was repeated 40 times, followed by a final extension period of 10 minutes at 72°C. The PCR product was self-ligated, and then transformed into *E. coli* DH5α by chemical transformation. Colonies were then selected and plasmid isolated using the QIAprep Spin

Miniprep Kit (Qiagen); restriction digestion was undertaken to ensure the correct construct (New England Biolabs).

For cloning of the overexpression vector, the region of the *Vc-nhaP2* gene corresponding to the predicted C-terminal tail was amplified to include XhoI and NdeI restriction sites. The PCR program involved a 30 second initial denaturing at 98°C, after which the thermocycle program ran as follows: 10 second denaturing at 98°C, 30 second annealing at 63°C, and 15 second extension at 72°C. This cycle was repeated 40 times, followed by a final extension period of 10 minutes at 72°C. The PCR product was ligated with restriction-digested pET21(b)+ and then transformed into *E. coli* DH5α by chemical transformation. Colonies were then selected and plasmid isolated using the QIAprep Spin Miniprep Kit (Qiagen); restriction digestion was undertaken to ensure the correct construct (New England Biolabs). Plasmids with accurate restriction digestion patterns were sent to the University of Calgary Core Sequencing Unit for confirmation.

2.2. CLONING AND EXPRESSION OF Vc-NhaP2

Sequence data for *V. cholerae* were obtained from the Institute of Genomic Research (*http://www.jcvi.org*). The predicted *Vc-nhaP2* ORF was amplified by high-fidelity polymerase chain reaction (PCR) using as a template chromosomal DNA of *V. cholerae* O395-N1 and the following primer pair: forward primer VcNhaP2expF, 5'-GAGGAATAATAAGTGGACGCCGTTACGATTAAC-3' and reverse primer VcNhaP2expR, 5'-TTACTCCGCGCCTTCTTGTAGCTC-3'. It was then directly cloned into the pBAD-TOPO vector (Invitrogen) under control of the arabinose-induced promoter (P_{BAD}*);* the resulting construct was termed pVc-NhaP2. The forward primer

was designed to achieve expression of the protein without the addition of the N-terminal leader sequence that is usually introduced by this vector; the primer contains an in-frame stop codon and a translation re-initiation sequence, which consists of a ribosome-binding site and the first GTG of the protein. The reverse primer maintained the native stop codon of *Vc-nhaP2*.

Construction of the deletion mutant was done using the "around-the-horn" method of cloning. The forward primer, 5'-GAAAACCTGTATTTCCAAGGGAA GGGCGAGCTTGAAGG-3', was designed to amplify around the plasmid starting from the native stop codon of Vc-nhaP2. The reverse primer, 5'-AATCGGCTCCGG TTTTGGGGGCACTTC-3', was designed to amplify around the plasmid starting from the final predicted transmembrane amino acid. In this way, beginning with the previously constructed pVc-NhaP2, a construct was designed that excluded the predicted cytoplasmic tail region, termed pVc-NhaP2Body. Construction of the deletion mutant was done using the pET21b(+) vector. Primers were designed to amplify the genomic *nhaP2* gene from *V. cholerae* such that the gene had an XhoI recognition site on its 5' end and an NdeI recognition site on its 3' end; the primer sequences were 5'-CGCAAACGACTCGAGCTCGGCGCCTTC-3' (forward) and 5'-CTGGCTAAACATATGCTGCCCCCAAAAC-3' (reverse).

2.3. BACTERIAL STRAINS AND CULTURE CONDITIONS

The Na^+/H^+ antiporter-deficient strain of *E. coli* TO114 [F1 IN (*rrnD-rrnE*) *nhaA::*Km^R *nhaB::*Em^R *chaA::*Cm^R] was kindly provided by H. Kobayashi (Faculty of Pharmaceutical Sciences, Chiba University, Chiba, Japan)[53]. This strain (transformed

with various constructs) was used for growth experiments and inside-out sub-bacterial membrane vesicle assays unless otherwise noted. For cloning and plasmid construction, DH5α (*supE44 hsdR17 recA1 endA1, gyrA96 thi-1 relA1*) (U.S. Biochemical Corp.) was used as the host. Unless otherwise indicated, TO114 cells were grown aerobically at 37°C with vigorous aeration in LBK medium (modified Luria broth with KCl replacing NaCl)[54] supplemented with 100 μg/mL erythromycin, 34 μg/mL chloramphenicol, 30 μg/mL kanamycin, 100 μg/mL ampicillin, and 0.05% (w/v) arabinose.

For overexpression, *E. coli* BL21 transformed with pRARE2 (Novagen) were grown in LB supplemented with 34 μg/mL chloramphenicol and 100 μg/mL ampicillin overnight. 15 mL of this culture was inoculated into 500 mL of LB containing the above antibiotics and grown until the OD_{600} reached 0.4-0.5, approximately 2.5 hours. The cells were then induced by addition of 0.4 mM isopropyl β-D-1-thiogalactopyranoside (IPTG) and grown for 4 more hours. They were then pelleted, and the pellet was frozen at -80°C until used.

V. cholerae wild-type and isogenic deletion Δ*nhaP2* strain O395-N1 were obtained from the laboratory of Dr. C.C. Häse, Oregon State University[55].

2.4. ANALYSIS OF GROWTH PHENOTYPES

For growth analysis of *E. coli* TO114 or the *V. cholerae* strain VcΔNhaP2 transformants, LBB medium (noncationic L broth) was supplemented with antibiotics, arabinose (see above), and varying concentrations of NaCl. 60 mM Bis-Tris propane (BTP) hydrochloride was added and the pH adjusted to either 6.0 or 7.2. 100 μL of overnight preculture were added to 4 mL of medium and grown at 37°C for 18 hours with

vigorous aeration. Growth was then measured as the OD of the bacterial suspension at 600 nm. All experiments were done in triplicate.

2.5. ISOLATION OF MEMBRANE VESICLES FOR ASSAYS OF ANTIPORT ACTIVITY

TO114/pVc-NhaP2, TO114/pBAD, and TO114/pVc-NhaP2Body transformants were grown in LBK medium supplemented with 100 μg/mL erythromycin, 34 μg/mL chloramphenicol, 30 μg/mL kanamycin, 100 μg/mL ampicillin, and 0.05% arabinose. Cells were harvested at an OD_{600} of 1.5-1.8 and immediately used for isolation of inside-out membrane vesicles as described previously[56]. Briefly, overnight cultures of TO114 transformants were grown in LBK medium containing the above antibiotics. The following morning, 10 mL of the preculture was added to 1 L fresh medium. Expression of the various constructs was induced upon addition of 0.05% arabinose after ~ 1.5 hours, with the cultures harvested upon attaining an OD_{600} of between 1.5-1.8.

After being harvested, the cells were washed three times in buffer containing 140 mM choline chloride, 10% (w/v) glycerol, and 20 mM Tris-HCl (pH 7.5). After the final wash, the bacterial pellet was resuspended in the same buffer containing 1 mM 1,4-dithiothreitol (DTT), 1 μg/mL pepstatin A, 0.1 mM phenylmethanesulfonyl fluoride (PMSF) and approximately 5 mg/L DNase. The cells were lysed by two passes through a French press (Aminco) and the unbroken cells were pelleted at 12,000g for 10 minutes at 4°C in an SS34 rotor (Sorvall). Membranes were harvested at 184,000g in a Ti-70 rotor (Beckman) for 90 minutes at 4°C. The resulting membrane pellets were then resuspended and stored in the same buffer containing all the additions except DNase until the assay

for cation/proton antiport activity. 100 μL aliquots of the resulting membrane vesicles were flash-frozen in liquid nitrogen and stored at -80°C until used.

2.6. MEASUREMENT OF TRANSMEMBRANE ΔpH

Antiport activity was assessed in vesicles using the Acridine Orange (AO) fluorescence quenching-dequenching assay. A schematic representation of this method is shown in Figure 2. AO, when uncharged, can freely diffuse through the vesicle membrane. Ionization, however, prohibits this diffusion. Since AO fluoresces upon illumination, a net increase in AO concentration inside the vesicle will result in a decrease in measured fluorescence of the solution (quenching). In our experiments, respiration-dependent generation of ΔpH was initiated by the addition of 20 mM Tris-D-lactate, which was oxidized by membrane-bound lactate dehydrogenase. This results in the generation of an electrochemical H^+ gradient, which acidifies the interior of the vesicle, resulting in ionization of intravesicular AO and net AO uptake (quenching).

After addition of a cation, antiport activity (if present) will result in the efflux of H^+, hence deacidifying the interior of the vesicle. This leads to net efflux of AO, and a corresponding increase in detected fluorescence (dequenching). The ratio of dequenching to lactate-induced quenching of AO fluorescence is taken to be the measure of antiport activity.

For ΔpH measurements, aliquots of vesicles (200 μg of protein) were added to 2 mL of buffer containing 140 mM choline chloride, 5 mM $MgCl_2$, 10% (v/v) glycerol, 4 μM acridine orange, and 50 mM BTP-HCl adjusted to the indicated pH. Fluorescence was monitored in a Shimadzu RF-1501 spectrofluorophotometer (excitation at 492 nm

and emission at 528 nm). A cation concentration of 10 mM was used in the determination of the pH profile of activity, and concentrations of 0.05-100 mM were used in the determination of the half-maximal effective cation concentration (apparent K_m). The antiport activities are expressed as the percent restoration of lactate-induced fluorescence quenching. Each experiment was conducted in duplicate on at least two separate isolations of membrane vesicles.

2.7. ISOLATION AND PURIFICATION OF THE Vc-NhaP2 C-TERMINAL TAIL

E. coli Rosetta 2 was grown and protein overexpression was induced as described in section 2.3. The cell pellet from 1 L of culture was resuspended in 25 mL of 20 mM Na^+-Phosphate pH 8.0, 300 mM NaCl (Buffer A) and pelleted. The supernatant was discarded and the pellets were resuspended in 25 mL of Buffer A supplemented with 1 mM 1,4-dithiothreitol (DTT), 1 μg/mL pepstatin A, 0.1 mM phenylmethanesulfonyl fluoride (PMSF), and 0.5 mM benzamidine. The resulting suspension was passed through a French pressure cell three times at 1,000 psi. Inclusion bodies and unbroken cells were pelleted at 12,000g for 20 minutes in an SS34 rotor, and the supernatant was collected. The supernatant was ultracentrifuged at 184,000g for 1.5 hours in a Ti-70 rotor. The resulting supernatant was collected and added to approximately 7.5 mL of Ni^{2+}-nitrilotriacetic acid agarose resin (Qiagen) that had been pre-equilibrated in Buffer A; this mixture was incubated with gentle rotation at 4°C overnight.

All chromatography steps were carried out on an AKTA FPLC system (GE Healthcare). The resin was packed into a column and washed in 20 mM Na^+-Phosphate

Figure 2. Schematic representation of the Acridine Orange fluorescence quenching-dequenching assays used to measure antiport activity in vesicles. See text for details.

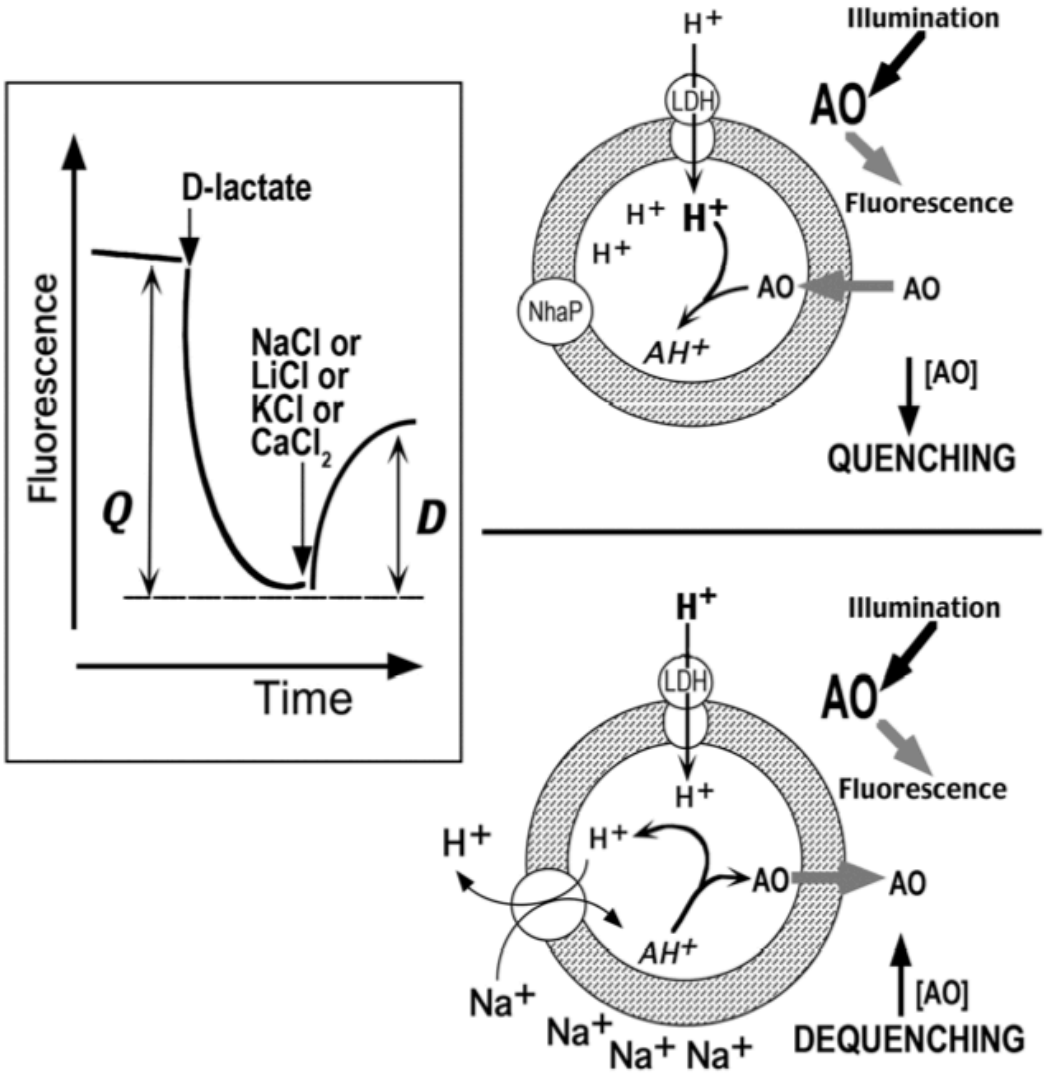

pH 7.0, 300 mM NaCl (Buffer B) until the A_{280} of the flowthrough returned to baseline. The protein was then eluted by a 0 - 1 M imidazole gradient in Buffer B. Fractions containing protein were collected and concentrated to approximately 1.2 mL using an Amicon Ultra 4 centrifugal filter with a molecular weight cutoff of 10,000 Da (Millipore).

The concentrated eluate was applied 350 µL at a time to a Superdex 75 size-exclusion column (GE Healthcare) pre-equilibrated with Buffer B. Peak fractions were collected, and the fractions containing the Vc-NhaP2 tail were confirmed with Western blotting and N-terminal sequencing (University of Iowa). Purity and homogeneity were confirmed by SDS-PAGE and dynamic light scattering (DLS) (see section 2.8 below). To check that the protein was correctly folded, circular dichroism (CD) spectroscopy was performed (see section 2.9 below).

Pure fractions were concentrated to approximately 1.0 mL using an Amicon Ultra 4 centrifugal filter with a molecular weight cutoff of 10,000 Da (Millipore) before adding 4 mL of 20 mM Tris-HCl pH 7.0, 300 mM NaCl (Buffer C). The sample was then concentrated to approximately 1.3 mL and stored at 4°C for further use. The concentration of the protein was determined using the DC Protein Assay (Bio-Rad).

2.8 DYNAMIC LIGHT SCATTERING

The homogeneity of the purified protein and its hydrodynamic characteristics were measured using a Nano-S Dynamic Light Scattering system (Malvern Instruments) as previously described[57]. Briefly, a 633 nm laser is passed through the protein sample; the time-dependent fluctuations in light scattering intensities yield the translational

diffusion coefficient of the particle. This parameter is related to the hydrodynamic radius of the particle via the Stokes-Einstein equation, which is calculated by the DLS software. The purified protein was diluted to 0.5 mg/mL with the appropriate buffer and passed through a 0.1 μm centrifugal filter (Millipore). 150 μL of the sample was then added to a 3 mm quartz cuvette. Prior to each measurement, the system was equilibrated to 20°C for 3 minutes. All measurements were done five times in succession.

2.9. CIRCULAR DICHROISM SPECTROSCOPY

CD measurements were done at protein concentrations of 0.230 mg/mL and 0.143 mg/mL on a Jasco J-810 CD spectropolarimeter (Jasco) in a quartz cuvette with a 0.5 cm path length. Purified protein was diluted to the desired concentration by addition of 12.5 mM Na^+-Phosphate pH 7.2, 200 mM NaF. Sample temperature was maintained at 20°C by a Julabo F25 circulating water bath. CD measurements were carried out in triplicate at 20°C between 250-190 nm UV light.

2.10. CRYSTALLIZATION TRIALS

Crystallization experiments were performed at a protein concentration of 5 mg/mL and 10 mg/mL in buffer C, at both 20°C and 4°C using the sitting drop method. For 48-well trays, 200 μL of mother liquor was deposited in the reservoir, and drops were made by mixing 1 μL of protein with 1 μL of mother liquor. For 96-well trays, the same procedure was followed with the exception that 100 μL of mother liquor was deposited in the reservoir. The trays were checked every few days for crystal growth.

For this study the commercial screens Crystal Screen 1, Crystal Screen 2, Index 1, and Index 2 (Hampton Research) and JB Classic 1-7 and 9, JBSG 1-4 (Jena Biosciences) were used.

3. Results

3.1. GROWTH PROFILE OF THE Vc-NhaP2Body TRUNCATION MUTANT

As described above, growth experiments were conducted involving antiporterless *E. coli* transformed with either pBAD, pVc-NhaP2, and pVc-NhaP2Body. Experiments were conducted in LBB broth containing the appropriate antibiotics at varying concentrations of NaCl at pH 7.2. Growth was measured as the OD600 after 18 hours of aerobic growth. The results for each strain are plotted in Figure 3.

Cells of *E. coli* TO114 are hypersensitive to Na^+ at pH 7.0 and higher[58]. At pH 7.2, ΔpH on the membrane is virtually nonexistent. Therefore, the presence of a functional antiporter will allow external Na^+ to move down its concentration gradient into the cell. As such, the presence of a functional antiporter will inhibit growth in this experimental system.

In our experiments, NaCl added at 200 mM to the LBB-based medium (pH 7.2) completely inhibited growth of TO114 transformed with "empty" pBAD24 vector (Fig. 3, empty bars). Interestingly, the TO114 cells expressing the full-length Vc-NhaP2 were much more sensitive to NaCl (Fig. 3, black bars), while the same cells expressing truncated Vc- NhaP2 grew as the "empty" host (Fig. 3, grey bars). At pH 6.0 neither full-length nor truncated Vc-NhaP2 affected the sensitivity of TO114 to NaCl (data not shown). These results suggest that the Vc-NhaP2 C-terminal tail plays a role in Na^+/H^+ antiport activity of Vc-NhaP2.

Figure 3. Growth phenotypes of the antiporter-less E. coli strain TO114 expressing full-length or truncated variant of Vc-NhaP2. Cells transformed with "empty" vector (pBAD24, open bars), expressing the full-length antiporter (pVc-NhaP2, black bars) or its truncated variant (pVc-NhaP2Body, grey bars) were grown aerobically in LBB medium (pH 6.0) supplemented with antibiotics, arabinose (0.0005% w/v) and indicated concentrations of NaCl for 18 hours. Plotted are the averages of two separate experiments, each performed in triplicate. Bars show the standard deviation.

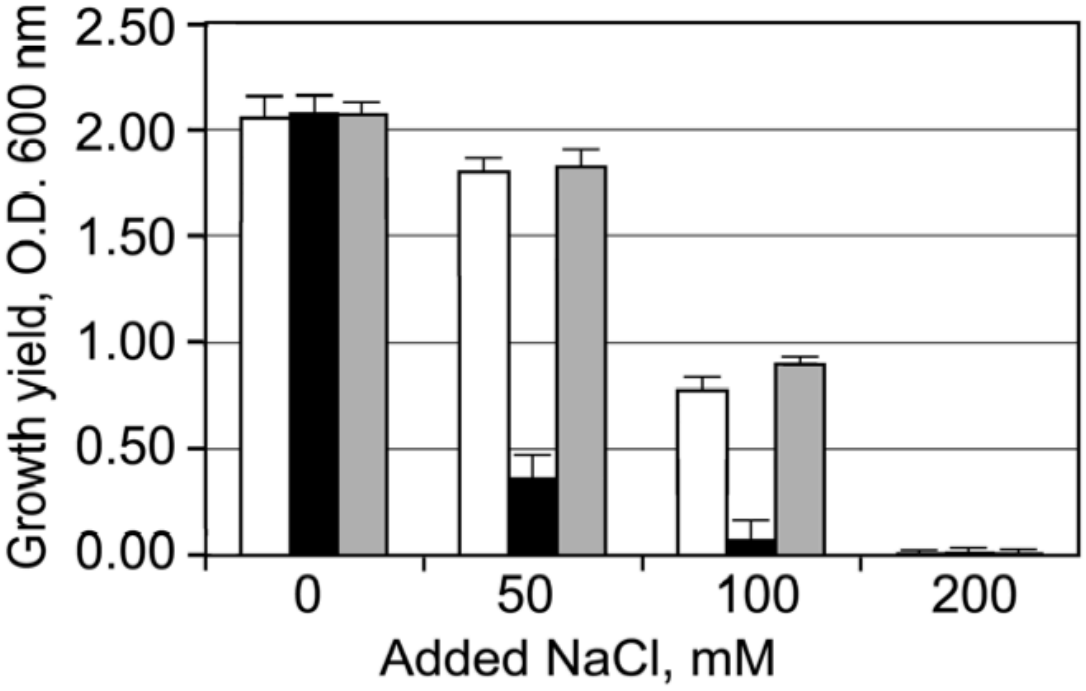

Growth experiments using the VcΔNhaP2 strain of *V. cholerae* were conducted in LBB broth containing 100 μg/mL carbenicillin and 100 μg/mL streptomycin, 0.0002% arabinose and supplemented with either 45 mM K^+ and 450 mM K^+, at pH 6.0. Cell growth was measured every hour as the OD_{600} of the culture. The results are summarized in Figure 4.

Chromosomal deletion of *Vc-nhaP2* in *V. cholerae* results in hypersensitivity to 400-500 mM K^+ at pH 6.0[59]. This phenotype can be complemented by expression of Vc-NhaP2 from a plasmid. We found that expression of truncated Vc-NhaP2 was sufficient to complement the deletion mutant's K^+-sensitive phenotype at pH 6.0. This shows that K^+/H^+ antiport activity can still occur in the absence of the C-terminal tail.

3.2. ION SPECIFICITY OF THE TRUNCATION MUTANT

Inside-out membrane vesicles from *E. coli* TO114 transformed with pVc-NhaP2 and pVc-NhaP2Body were prepared as described above. These vesicles were used to compare antiport activity of the wild-type and truncated Vc-NhaP2 using the Acridine Orange fluorescence quenching-dequenching assay previously described (see Figure 2). Each point plotted in Figure 5 represents the average AO fluorescence dequenching measured for either substrate cation at a given pH. As Figure 5 shows, the K^+/H^+ antiport mediated by truncated Vc-NhaP2 was significantly less efficient than that for wild-type Vc-NhaP2. Furthermore, Na^+/H^+ antiport was effectively abolished at all pH values tested. Thus, deletion of the C-terminal tail markedly decreases the efficiency of antiport for both substrate cations. These results suggest that the Vc-NhaP2 C-terminal tail plays a role in both K^+/H^+ and Na^+/H^+ antiport.

Figure 4. Growth curves of the VcΔNhaP2 strain of *V. cholerae* in medium containing K^+. At lethal concentrations of K^+ (450 mM), the uncomplemented mutant dies. The truncated version of Vc-NhaP2 is sufficient to allow for normal growth under these conditions. In medium containing K^+ concentration close to intracellular levels, the uncomplemented mutant's growth lags, but it does not die.

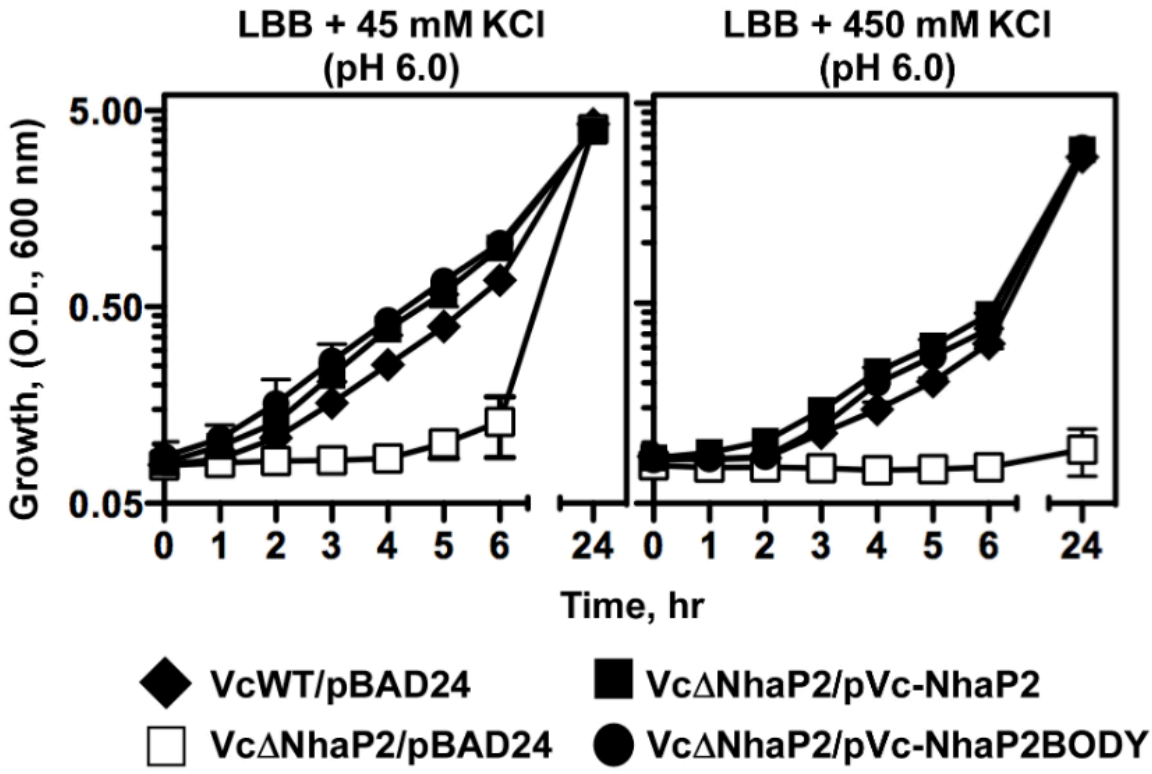

Figure 5. pH profile of antiport activity for Vc-NhaP2 and the Vc-NhaP2Body for K^+ and Na^+. Each point on the plots represents the average of all Acridine Orange fluoresence dequenching measurements taken at the indicated pH for the indicated cation (an example of such a measurement is shown in Figure 5B). Error bars represent the standard deviation for each measurement. For K^+, antiport activity is significantly reduced by truncation of the C-terminal tail at pH 9.0 and below. For Na^+, antiport activity is significantly reduced and essentially abolished at all pH values.

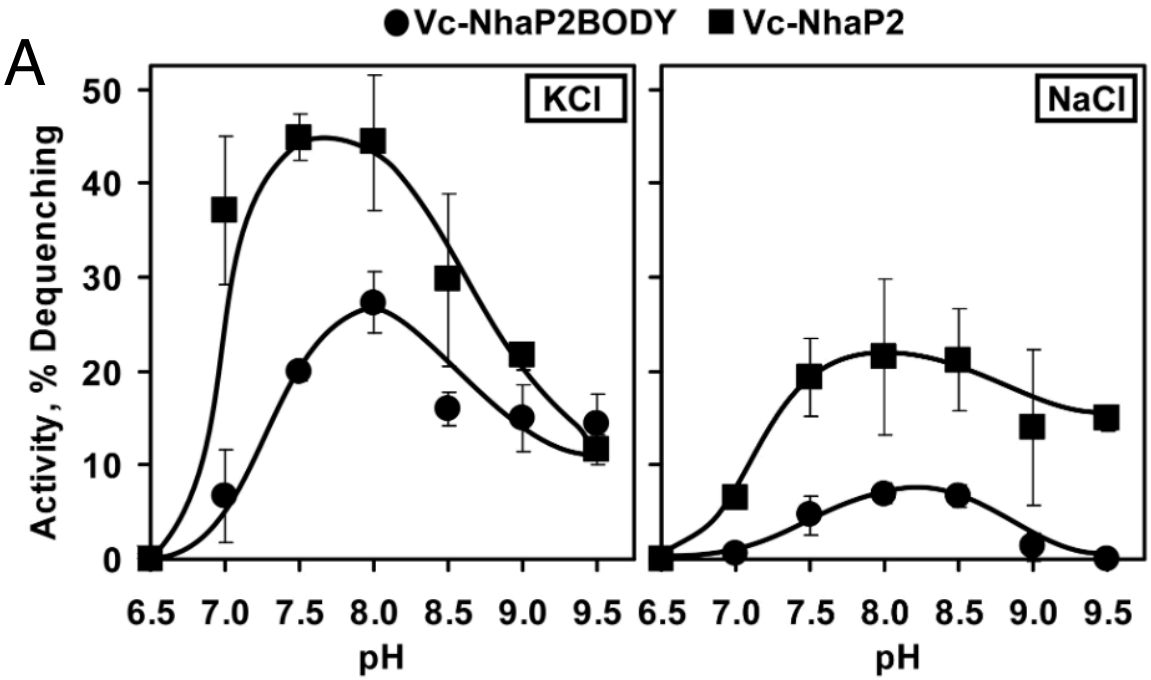

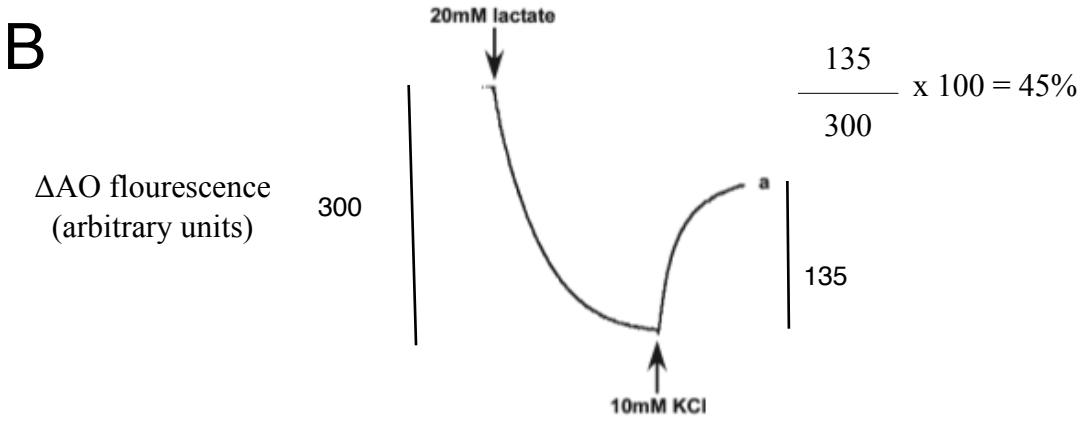

pH = 7.5, Vc-NhaP2

3.3. KINETIC PROFILE OF THE TRUNCATION MUTANT

The same inside-out membrane vesicle assays were conducted to generate kinetics plots for the Vc-NhaP2Body. By convention, the substrate concentration at which antiport activity as registered by fluorescence dequenching is half-maximal is regarded as the apparent K_m of the antiporter for that substrate[60,61,62]. This serves as a convenient measure of the affinity of the antiporter for a given substrate cation. Data were collected at pH 7.5 at varying levels of K^+ and the apparent K_m was determined from these data using the Prism 4.0 software (GraphPad) for K^+ at pH 7.5. As shown in Figure 6, deletion of the C-terminal tail resulted in an approximately 5-fold increase in the apparent K_m for K^+. The K_m for K^+ at pH 7.5 was found to be 25 mM for truncated Vc-NhaP2; the K_m for wild type Vc-NhaP2 calculated by the same method under these conditions was determined to be 5 mM. These results indicate that deletion of the C-terminal tail reduces the affinity of Vc-NhaP2 for its major substrate, K^+; this, in turn, clearly suggests that the C-terminal tail is involved in antiport.

3.4. RECONSTITUTION OF ANTIPORT ACTIVITY IN THE TRUNCATION MUTANT

Reconstitution assays were carried out using a modified protocol to that used by Waditee et al. (2006). Briefly, 100 μg of purified tail peptide was mixed with 200 μg of vesicles. The mixture was incubated on ice for 15 minutes; it was then assayed exactly as described in section 2.6. As controls, purified tail was added in the same way to vesicles expressing full-length Vc-NhaP2. Also, a 25 kDa β-lactamase purified in the same way as the Vc-NhaP2 tail was added in its place. Neither control treatment affected the

Figure 6. Michaelis-Menten plot for Vc-NhaP2 and Vc-NhaP2Body at pH 7.5. Calculation of the apparent K_m from these data indicates that truncation of the C-terminal tail decreases affinity for K^+ by five times.

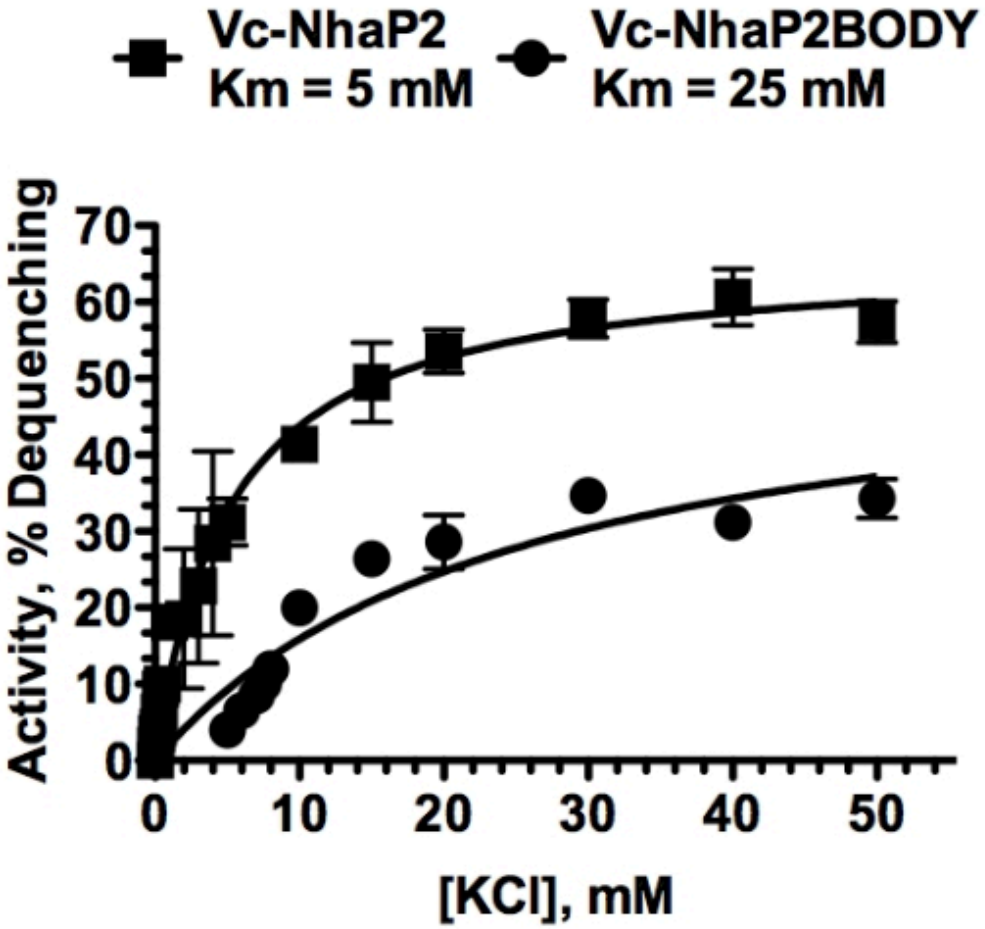

experiment in any way, and these results are omitted from Figure 7. The results of the experiment comparing vesicles overexpressing Vc-NhaP2, the Vc-NhaP2Body, and the Vc-NhaP2Body with added C-terminal tail are summarized in Figure 7.

As is evident in the figure, addition of the purified C-terminal tail back to vesicles expressing the Vc-NhaP2Body alone significantly increased its antiport activity at most of the pH values tested. The greatest level of reactivation observed was in the pH range of 7.5-8.5. This is further evidence that the C-terminal tail of Vc-NhaP2 is involved in antiport.

3.5. PURIFICATION OF THE C-TERMINAL TAIL

The C-terminal tail of Vc-NhaP2 was successfully purified using a two-step protocol. The first purification step was performed on a Ni^{2+}-NTA column. Figure 8 shows the A_{280} elution profile of the protein. It shows that partially pure protein eluted between 250-500 mM imidazole, indicating that the 6xHis tag successfully bound to the Ni^{2+}-NTA column. Subsequently, an SDS-PAGE gel of each fraction was run to assess the degree of purity of the eluate. An image of the gel is shown in Figure 9. It showed that the protein eluted from the Ni^{2+}-NTA column was not entirely pure and that a second purification step was needed.

As outlined above, final purification of the C-terminal was achieved by size-exclusion chromatography using a Superdex75 column. The protein eluted at a volume of 10.9 - 11.1 mL, which corresponds to a protein with a molecular weight of ~ 34,000 Da. The monomeric weight of the protein is ~ 25,000 Da, which suggests that the protein as eluted is probably monomeric (see Figures 10).

Figure 7. Reconstitution of antiport activity in vesicles expressing the Vc-NhaP2Body upon addition of purified C-terminal tail. Addition of purified C-terminal tail to vesicles expressing Vc-NhaP2 and addition of 25 kDa β-lactamase to vesicles expressing the Vc-NhaP2Body were used as controls (data not shown). Addition of the tail to vesicles expressing the Vc-NhaP2Body significantly increased antiport activity.

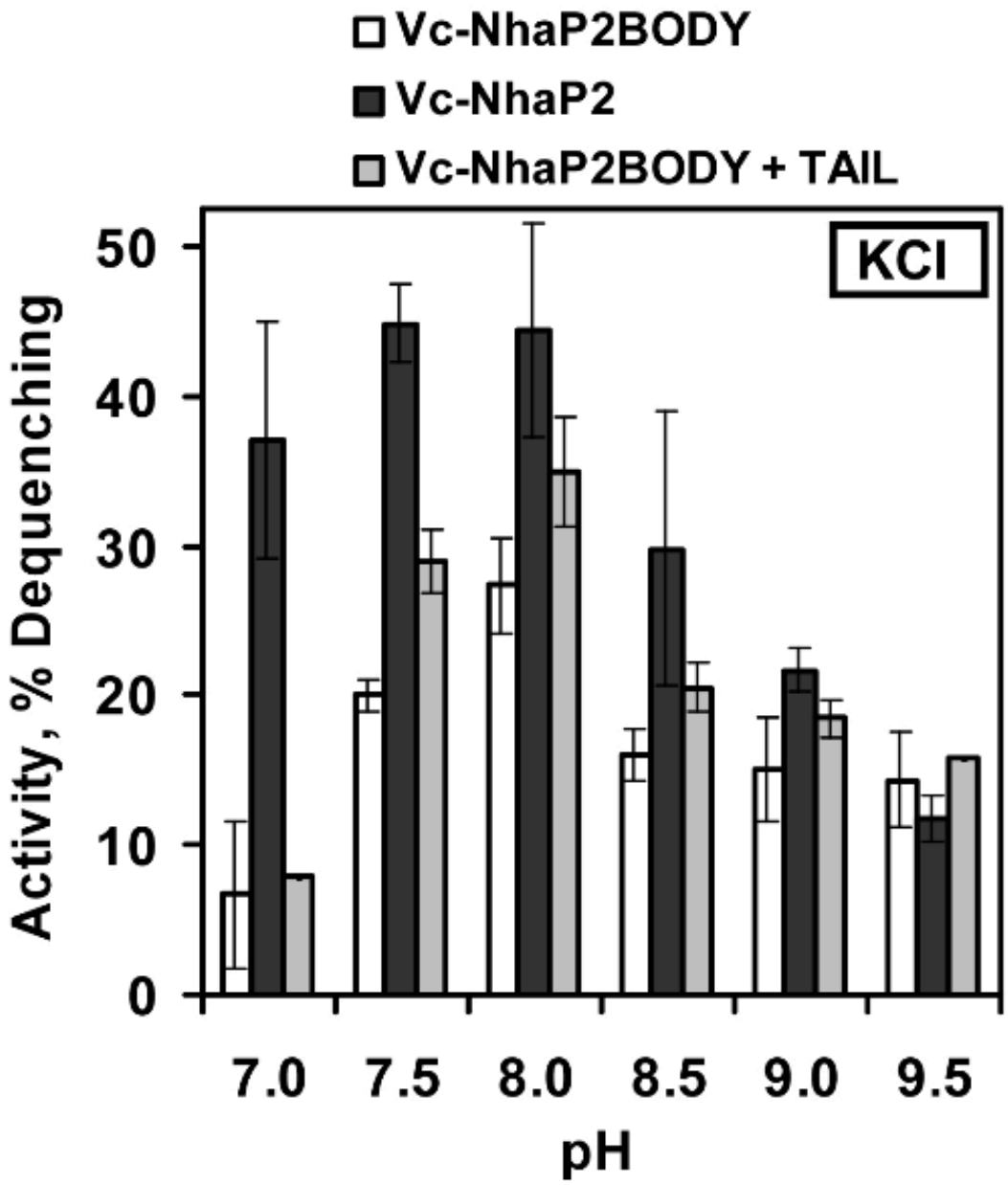

An initial peak that eluted between ~ 7.5 - ~9.5 mL represented protein that was larger than the column limit of 75,000 Da. Of note, SDS-PAGE and Western blotting showed that some Vc-NhaP2 tail was present in the void. This represents higher oligomeric or aggregate states of the protein.

An SDS-PAGE gel was run to assess the purity of the protein (Figure 11). Although there are two bands in fractions B6 and B7, both bands were confirmed by Western blot and N-terminal sequencing to be the Vc-NhaP2 tail. The 50 kDa band likely represents a very strongly associated dimer which could not be resolved by the denaturing conditions employed.

Figure 8. Elution profile of cleared supernatant after application to the Ni^{2+}-NTA resin. Elution was done by imidazole gradient (diagonal line); the protein eluted between 250-500 mM imidazole. The y-axis represents the A_{280} of the solution.

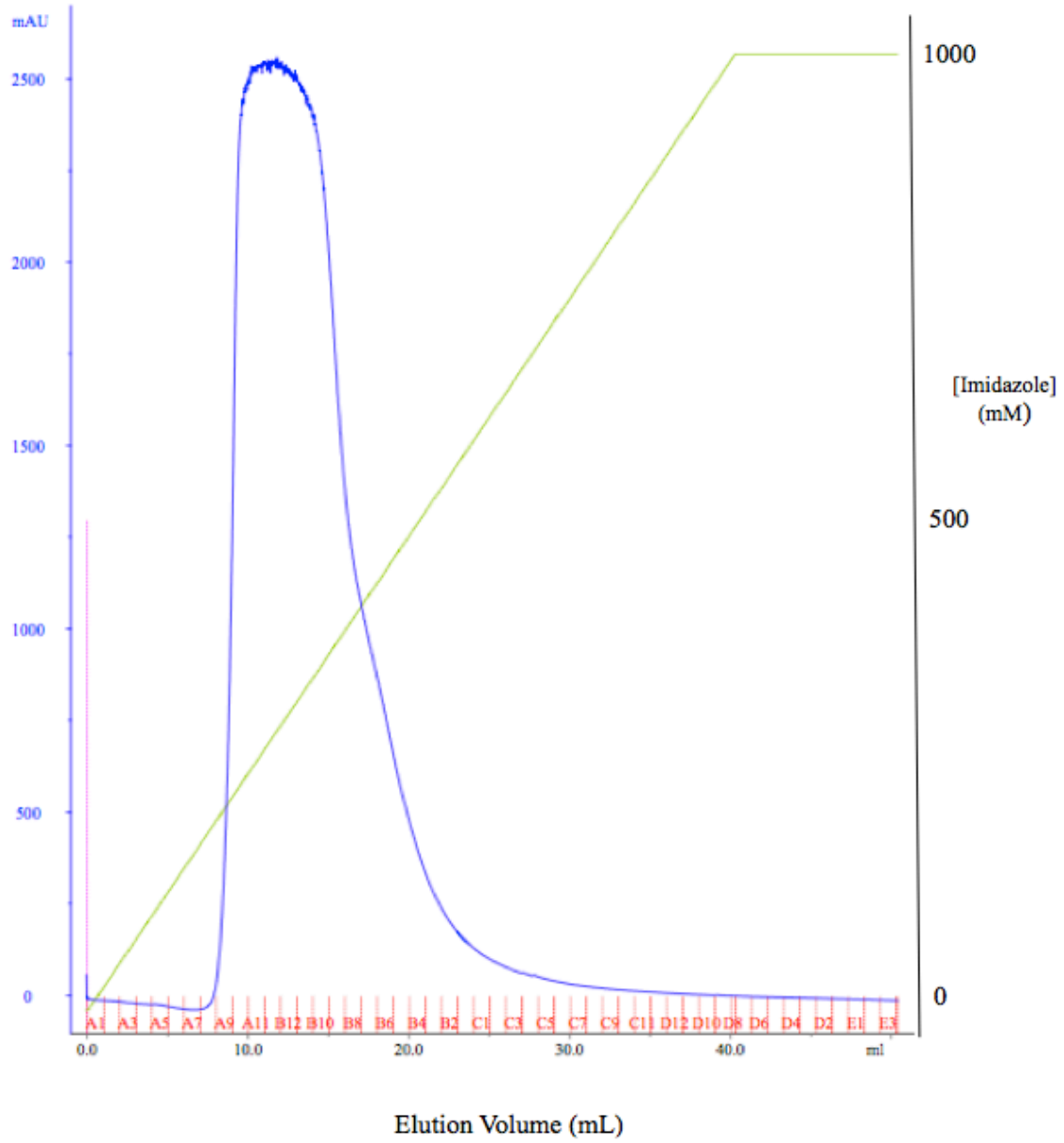

Figure 9. SDS-PAGE gel showing the cell lysis insoluble fraction (I), soluble fraction (S), flow-through upon pH 7.0 wash (FT1 and FT2) and fractions corresponding to elution profile in Figure 8. The major bands at approximately 25 kDa and 50 kDa represent monomeric and dimeric Vc-NhaP2 tail, respectively, confirmed by Western blot and N-terminal sequencing.

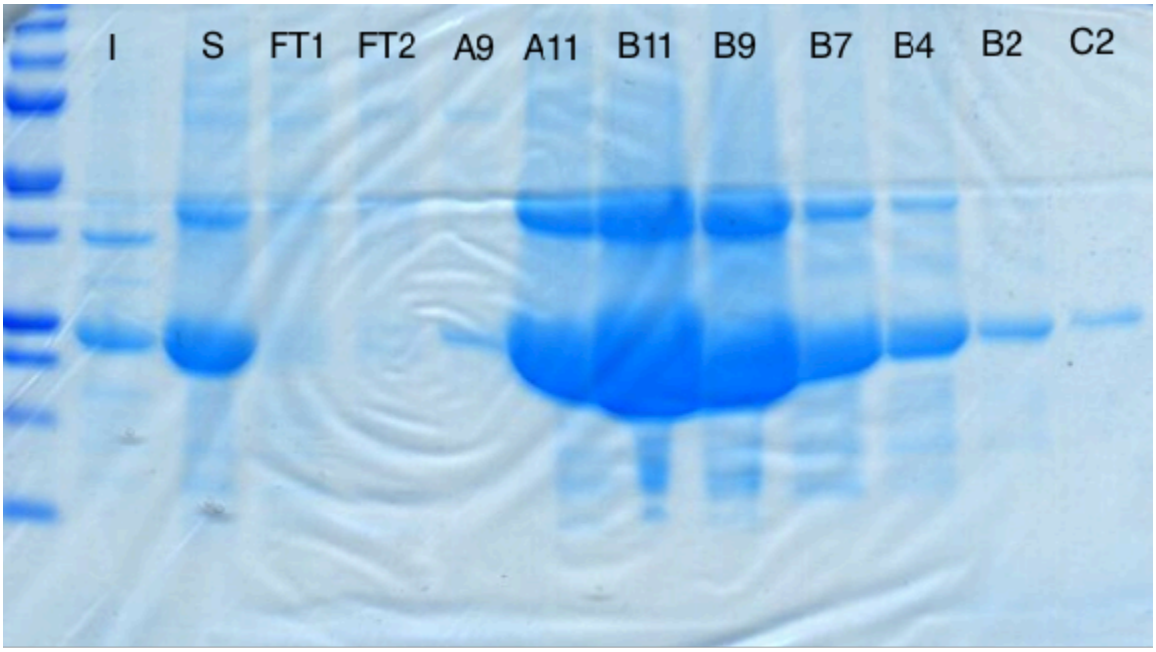

Figure 10. Elution profile of fractions collected following Ni^{2+}-NTA chromatography upon application to the Superdex75 size-exclusion resin. The first peak represents the void, containing any protein larger than 75 kDa. This includes undesired protein as well as some oligomerized C-terminal tail. The second peak represents pure Vc-NhaP2 tail; it elutes at a molecular weight of approximately 35 kDa. The y-axis represents the A_{280} of the solution.

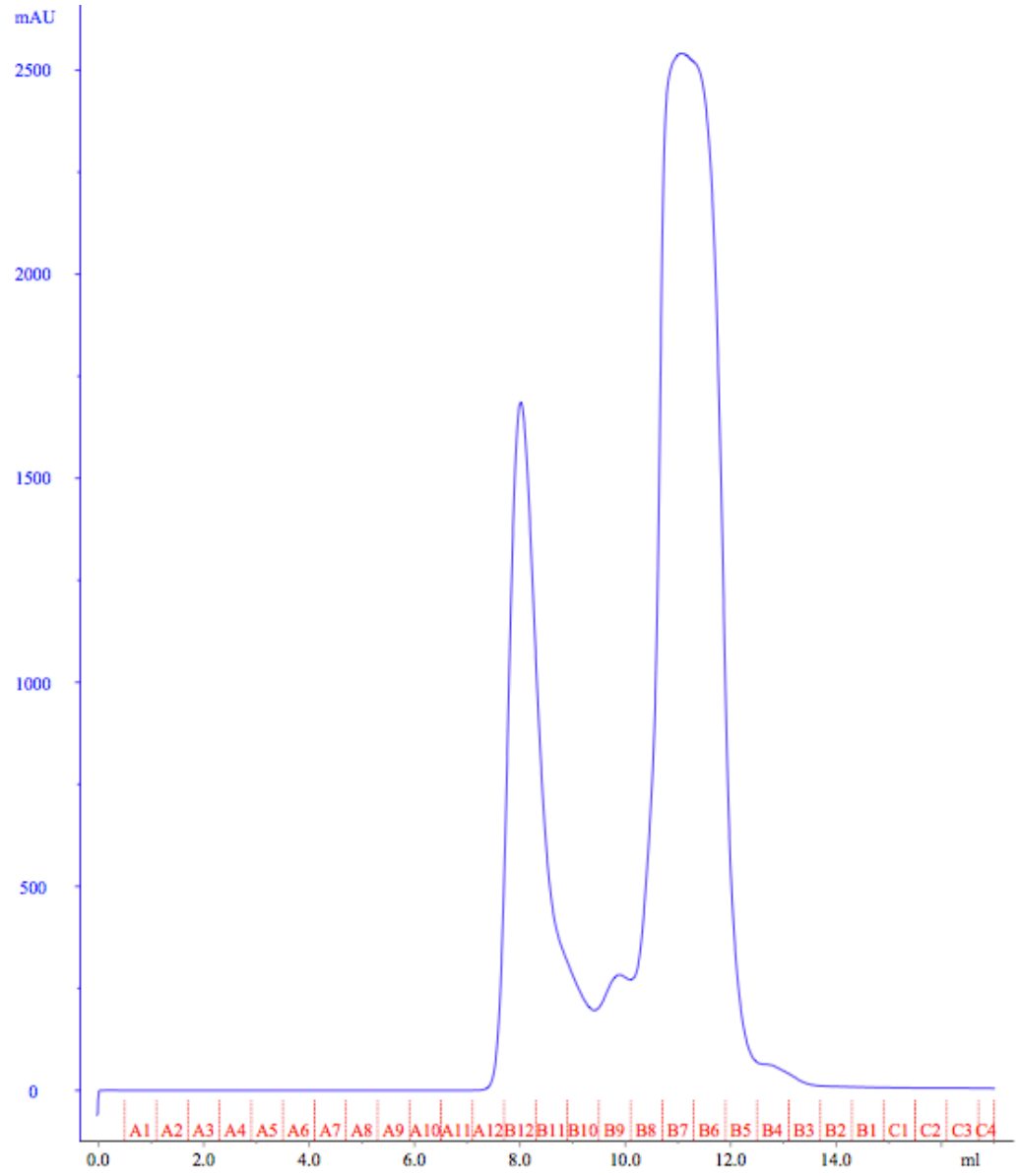

Elution Volume (mL)

Figure 11. SDS-PAGE gel following Superdex75 chromatography. The concentrated Ni^{2+}-NTA fractions are shown in the leftmost lane (SM), followed by fractions corresponding to those in Figure 10. Fractions B7 and B6 were collected and concentrated; identity of the bands as the Vc-NhaP2 tail was confirmed by Western blot and N-terminal sequencing, and purity of the fractions was confirmed by DLS. The 25 kDa band represents monomeric Vc-NhaP2, and the 50 kDa band the dimeric form.

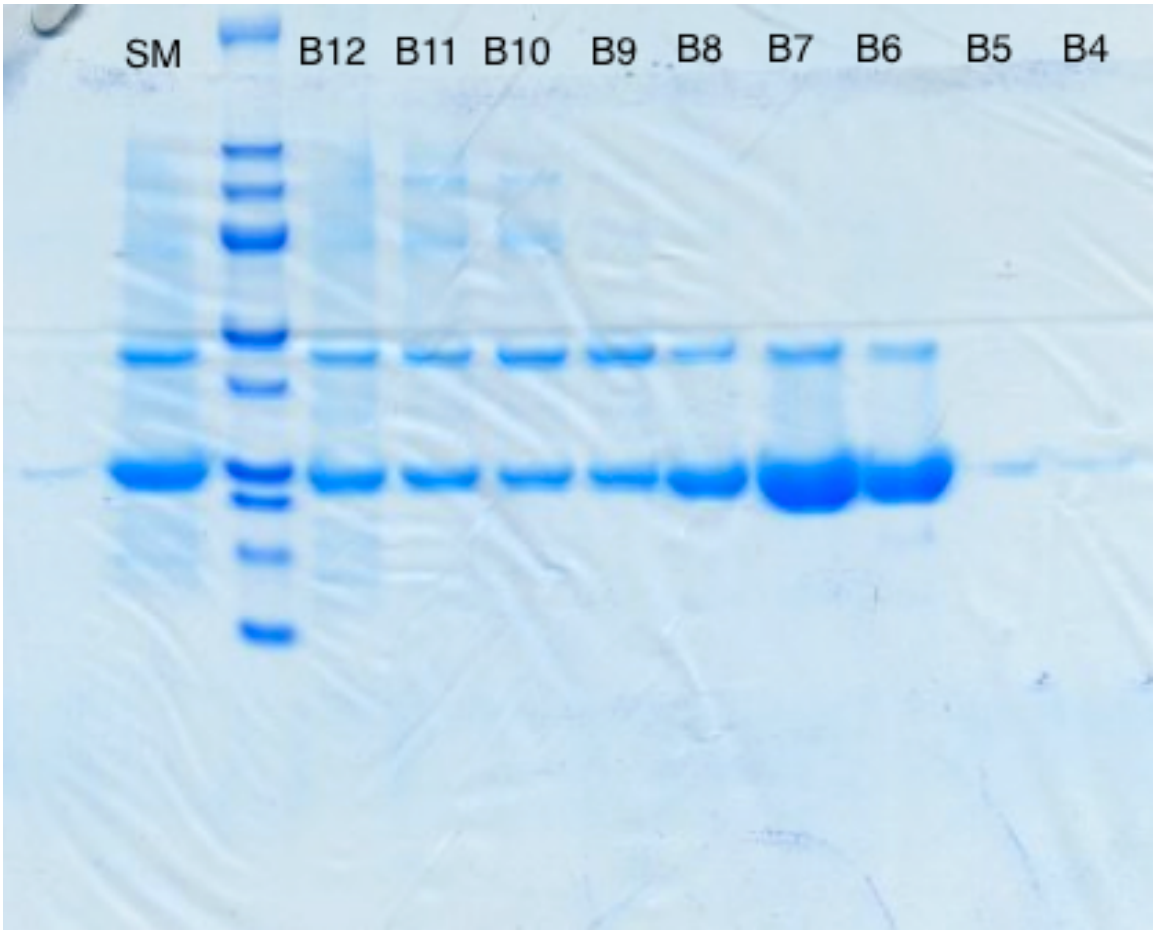

3.6. DYNAMIC LIGHT SCATTERING

Figure 12 shows the results of dynamic light scattering performed on the purified Vc-NhaP2 tail at a concentration of 0.5 mg/mL in a buffer containing 20 mM Tris-HCl pH 7.0, 300 mM NaCl. Our light scattering results showed a single species whose hydrodynamic radius changed in each subsequent measurement; specifically, it ranged from ~ 2 nm to ~ 6 nm. This suggests a dynamic between oligomeric states in an otherwise homogenous sample.

At lower pH values, this dynamic equilibrium becomes more apparent still (Figure 13). However, if the pH was lowered to 5.0, which is close to the pI of the protein (~ 4.5), the protein formed large aggregates, evidenced by the fact that all five measurements were > 1,000 nm in size (Figure 14). To see if the ionic strength of the buffer influenced these fast dynamic transitions, we lowered the NaCl concentration from 300 mM to 100 mM and raised it from 300 mM to 1 M NaCl. The results of these experiments are shown in Figures 15 and 16; the data collected showed that neither ionic strength of the buffer or pH influenced this behavior.

Given the predicted presence of a Rossman fold, FAD was added to the experimental buffer to determine whether it had an effect on protein behaviour in solution. 10 μM FAD was added to the pH 7.0 buffer in Figure 12 to see if the presence of the cofactor would stabilize the protein in a single oligomeric form (Figure 17). This resulted in a homogenous species whose radius was ~ 3 nm.

Taken together, these DLS results indicate that the C-terminal tail exhibits dynamic oligomerization in solution, a behavior which is stabilized by addition of FAD.

This suggests that FAD interacts with the protein, and further hints that the predicted Rossman fold is indeed present.

3.7. CIRCULAR DICHROISM SPECTROSCOPY

A CD spectrum of the C-terminal tail between 190 and 250 nm was successfully determined (Figure 18). The resultant spectrum was characteristic of a folded protein with two minima observed at 208 nm and 222 nm, which is typical for proteins which contain some α-helical structure. Most importantly, this CD spectrum is clearly not indicative of the isolated protein being made up exclusively of random coil. This result is in agreement with the GOR (ExPASy) prediction, which predicted the C-terminal tail to be approximately 40% α-helical.

3.8. CRYSTALLIZATION TRIALS

At the time of this writing, a number of potential conditions for crystal growth have been identified. Of these, we tried to mount the two most promising conditions to determine if they were protein or salt. The first crystal was from Crystal Screen 2 (Hampton Research), condition number 27, which contained 100 mM MES pH 6.5, 10 mM $ZnSO_4 \cdot 7H_2O$, 25% PEG 500. Unfortunately, the crystals were too fragile to be mounted, but addition of methylene blue to the crystal fragments showed the crystals to be protein. Therefore, we hope to be able to optimize this condition to the point where data can be collected in the future. The second crystal was grown with JBSG 3 (Jena Biosciences) condition number B2, which consisted of 100 mM Na^+-Acetate pH 4.6, 1 M $(NH_4)_2HPO_4$, and this was shown to be a salt crystal.

Figure 12. DLS plot showing the average hydrodynamic radius of C-terminal tail in 20 mM Tris-HCl pH 7.0, 300 mM NaCl. Measured hydrodynamic radii range from ~ 2 nm to ~ 6 nm. Each peak represents the result of individual but subsequent measurements.

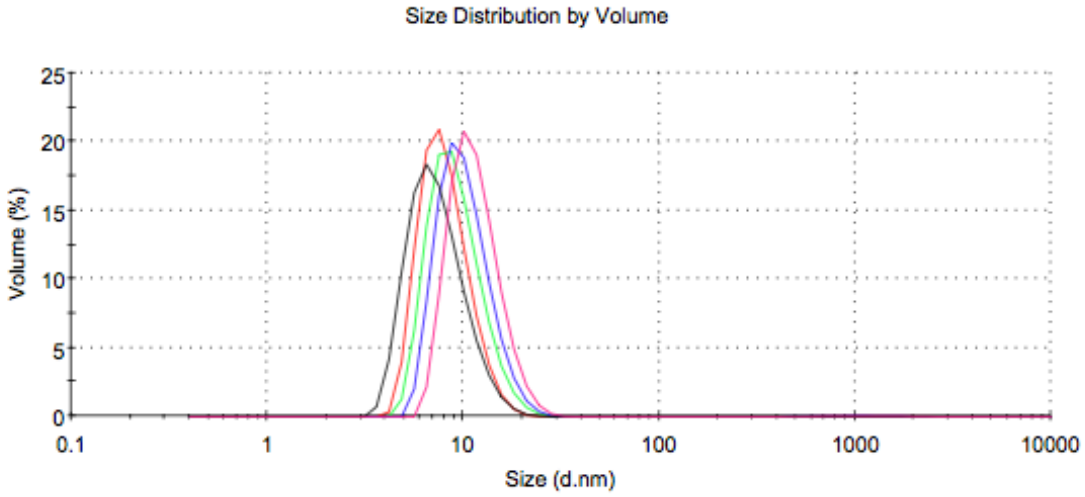

Figure 13. DLS plot showing the average hydrodynamic radius of C-terminal tail in 20 mM Na^{+}-Citrate pH 6.0, 300 mM NaCl. Measured hydrodynamic radii range from ~2 nm to ~6 nm. Each peak represents the result of individual but subsequent measurements.

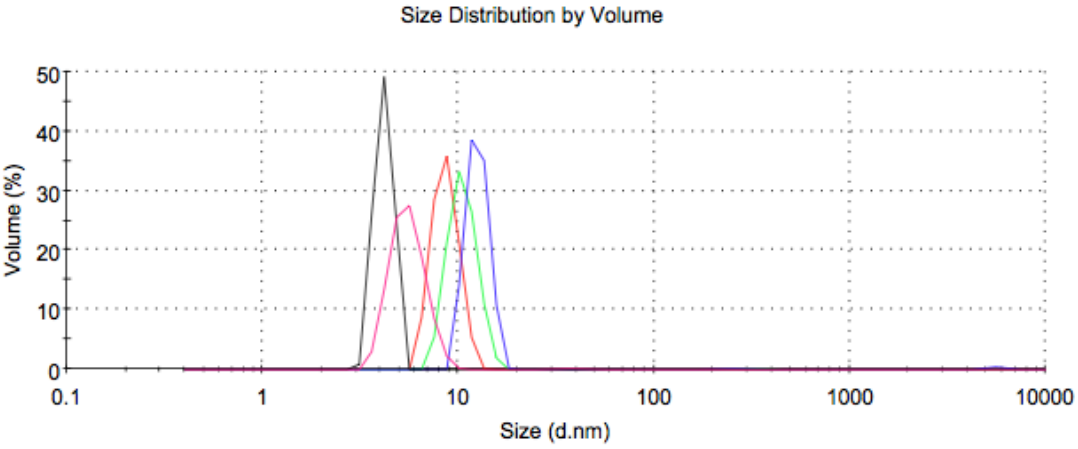

Figure 14. DLS plot showing the average hydrodynamic radius of C-terminal tail in 20 mM Na^{+}-Acetate pH 5.0, 300 mM NaCl. These data show aggregation of the protein. Each peak represents the result of individual but subsequent measurements.

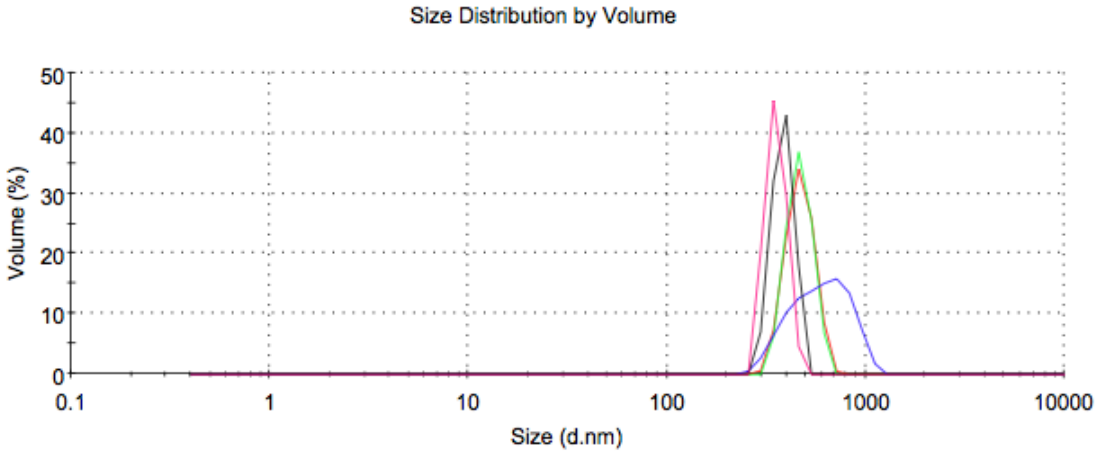

Figure 15. DLS plot showing the average hydrodynamic radius of C-terminal tail in 20 mM Tris-HCl pH 7.0, 100 mM NaCl. These data show the presence of various oligomeric states. Each peak represents the result of individual but subsequent measurements.

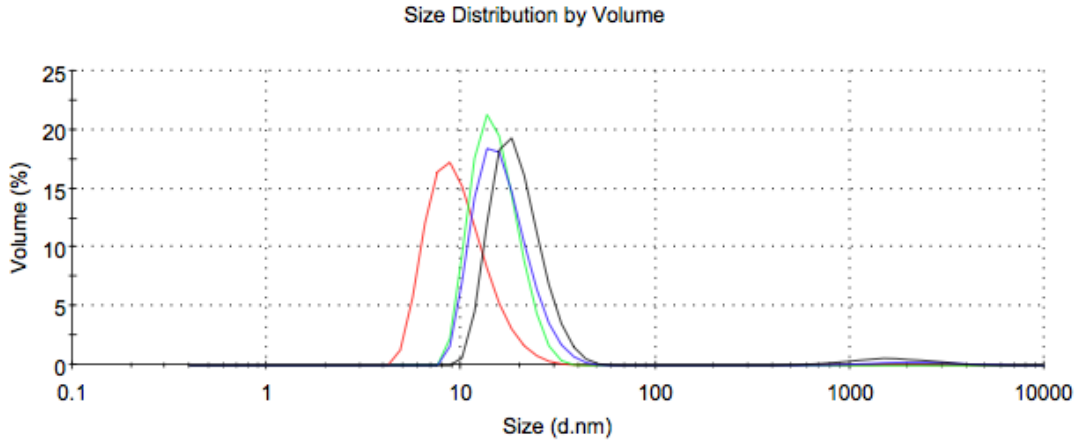

Figure 16. DLS plot showing the average hydrodynamic radius of C-terminal tail in 20 mM Tris-HCl pH 7.0, 1 M NaCl. These data show the presence of various oligomeric states. Each peak represents the result of individual but subsequent measurements.

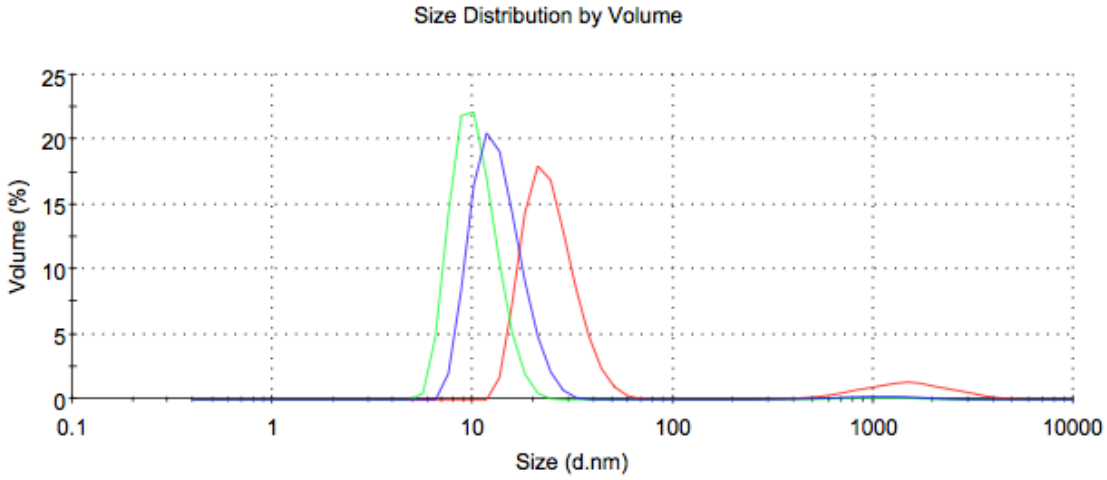

Figure 17. DLS plot showing the hydrodynamic radius of C-terminal tail in 20 mM Tris-HCl pH 7.0, 300 mM NaCl, 10 µM FAD. These data show the presence of a single species, ~ 3 nm in radius. Each peak represents the result of individual but subsequent measurements.

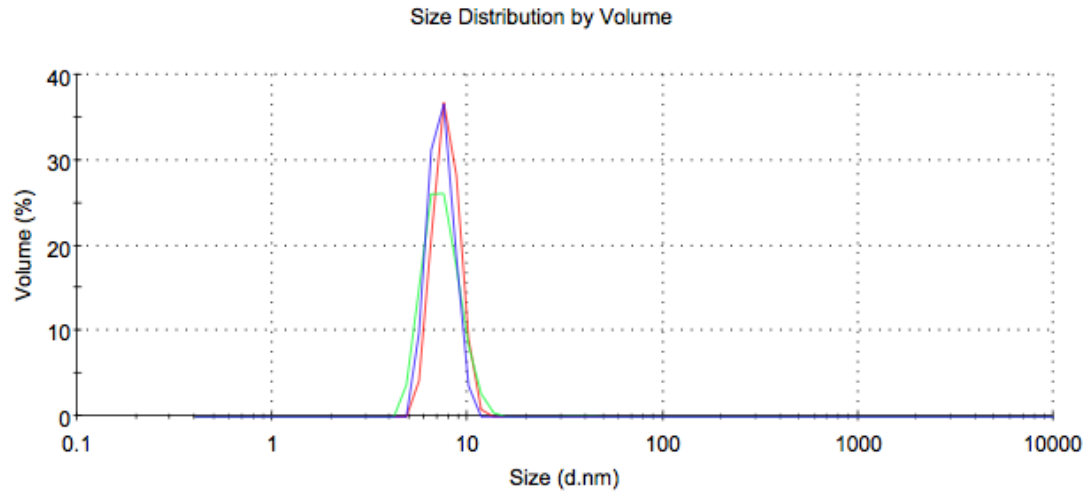

Figure 18. CD spectrum of the C-terminal tail in 12.5 mM Na^+-Phosphate pH 7.2, 200 mM NaF. The spectrum is indicative of a folded protein containing some α-helical secondary structure.

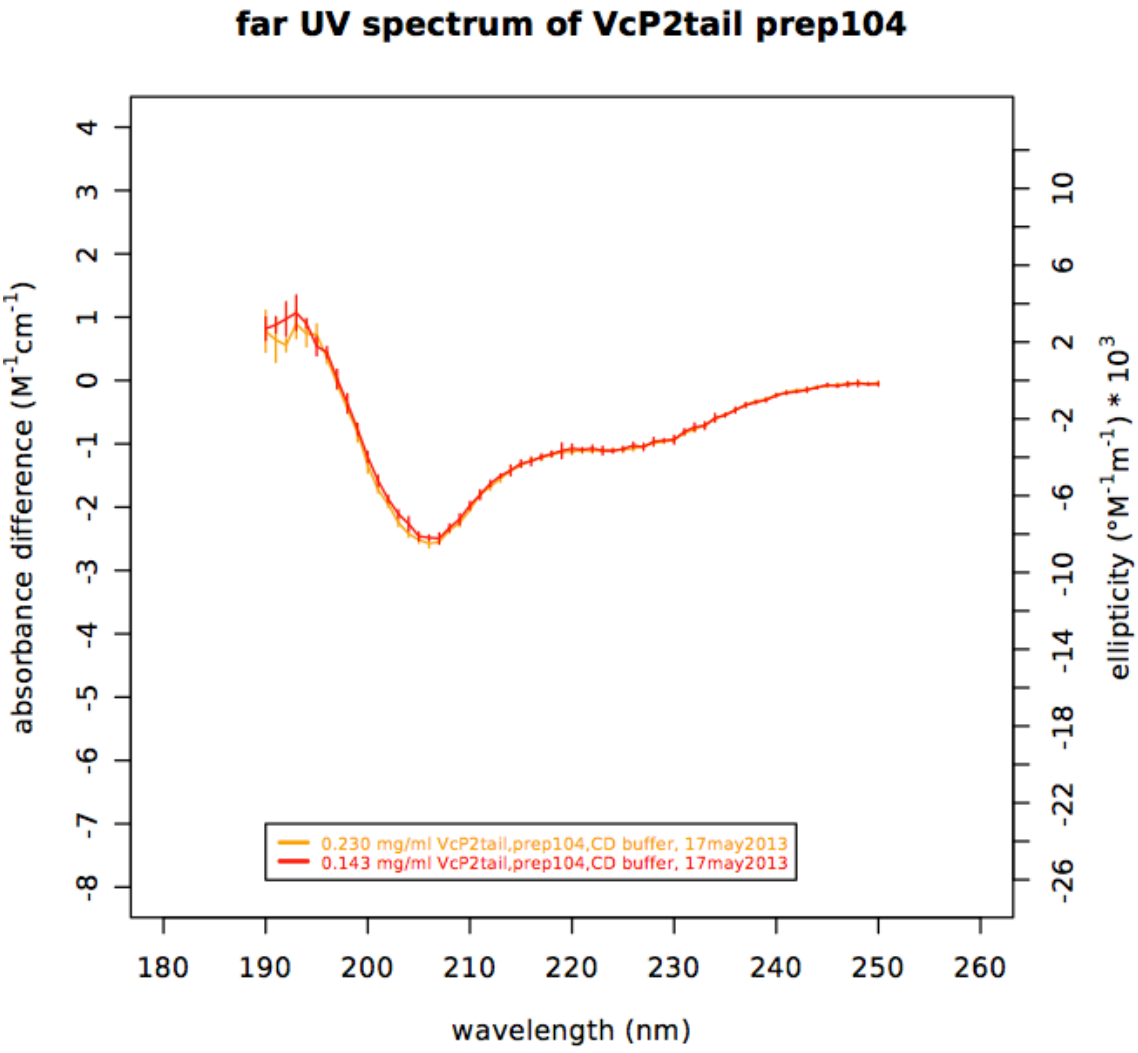

4. Discussion

4.1. GROWTH PROFILES OF DELETION MUTANT

In medium of pH 7.2, cation/H^+ antiport mediated by an non-electrogenic antiporter, such as Vc-NhaP2, might be slightly reversed (i.e. inwardly directed) due to the absence of an inwardly directed pH gradient on the membrane[63]. Therefore, non-electrogenic antiporters are unable to extrude toxic cations from the cytoplasm at above neutral pH and, in fact, they may even weakly facilitate transport of cations into the cell. Conversely, a non-functional or partially functional antiporter will not transport cations into the cell and this will be manifested as a somewhat enhanced resistance to the toxic cation. Therefore, it would be expected that cells in such a medium overexpressing a functional antiporter will not be able to grow at NaCl concentrations of more than 50 mM, whereas cells overexpressing a functionless (or even a less active) antiporter will be able to grow. This is exactly what we observed (Figure 3) for antiporterless cells of *E. coli* transformed with "empty" vector, pBAD (i.e. not overexpressing a functional antiporter), which were able to grow with salt present in the medium. Conversely, as expected, the same cells transformed with pVc-NhaP2 and thus overexpressing the wild-type antiporter were unable to grow in the presence of salt. Cells overexpressing the Vc-NhaP2Body, which lacked the C-terminal tail, displayed the same growth profile as those transformed with pBAD. This result strongly hints that Vc-NhaP2 lacking the C-terminal tail has impaired Na^+/H^+ antiport activity, which is the first experimental evidence supporting a role of the C-terminal tail in ion transport catalyzed by Vc-NhaP2.

At pH 6.0, normal antiport (i.e. the extrusion of toxic Na^+ in exchange for H^+) would be restored. At this pH, the presence of a functional antiporter would not be expected to inhibit growth, since the proton gradient would drive extrusion rather than import of toxic cations. Indeed, as expected, at pH 6.0 growth was observed in the presence of salt in all cases. These results are in agreement with the hypothesis that deletion of the C-terminal tail reduces the function of the antiporter.

Data that we obtained clearly shows that the VcΔNhaP2 strain of *V. cholerae* overexpressing Vc-NhaP2Body grows at the same rate as wild type *V. cholerae* and VcΔNhaP2 overexpressing Vc-NhaP2 in medium containing K^+ (Figure 4). At a first glance, this seems to run contrary to the results showing that truncation of the C-terminal tail decreases efficiency of antiport and affinity for K^+. However, this could be explained in one of two ways. First, it is possible that even the low antiport activity of the Vc-NhaP2Body is sufficient to maintain normal growth. Second, given that the number of antiporters found in the membrane following overexpression vastly outnumbers constitutive expression of any antiporter by orders of magnitude, it is possible that the inefficient antiport of Vc-NhaP2 is easily compensated for by sheer number. Therefore, growth experiments of this type do not necessarily indicate the efficiency of antiport, but are simply able to show absence or presence of antiport.

4.2. ION SPECIFICITY OF THE Vc-NhaP2Body

Inside-out membrane vesicle assays measuring the percentage of acridine orange fluorescence dequenching (thereby measuring antiport activity) generated the pH profiles of Vc-NhaP2 activity shown in Figure 5. As can be seen, at pH 7.0 and pH 7.5, the Vc-

NhaP2Body variant exhibits less than 50% the antiport activity of the wild-type Vc-NhaP2. At all pH values measured, for both K^+ and Na^+, antiport is much less efficient in the truncation mutant than in wild-type Vc-NhaP2 up until pH 9.5, beyond which respiration would be impossible and the experimental system would cease to function. Of note, the Na^+/H^+ antiport catalyzed by Vc-NhaP2Body does not exceed 10% at any tested pH (Figure 5). Such marginal levels of sodium transport explain why cells of TO114 expressing Vc-NhaP2Body growing at neutral pH are as resistant to Na^+ ions as those containing "empty" vector.

These findings support the results of the growth experiments outlined above, which hint that the C-terminal tail is involved some way in antiport. The determination of the exact nature of this involvement, however, will be left to structural studies.

4.3. KINETIC PROFILE OF THE TRUNCATION MUTANT

The previously reported apparent /K_m of Vc-NhaP2 for K^+ at pH 7.5 is 1.62 mM[64]. However, the method used to determine this value was the slope-intercept method (i.e. linear regression) which, for statistical reasons[65], is not the most accurate method for determination of the Michaelis constant. Therefore, the Prism 4.0 software, which uses non-linear regression, was used for apparent K_m determination, yielding values of 5 mM and 25 mM for Vc-NhaP2 and the Vc-NhaP2Body, respectively. This represents a 5-fold decrease in affinity for K^+ in the truncated variant of the antiporter; this is perhaps the most compelling evidence thus far that the C-terminal cytoplasmic tail plays a role in antiport. It should be noted here that such an effect could not be attributed to impaired expression and/or targeting of Vc-NhaP2 as a result of the truncation. Indeed,

experiments conducted by C. Resch in our lab indicate that both variants of Vc-NhaP2 are present in membranes of *E. coli* TO114 cells in very similar amounts (C. Resch, personal communication). Whether the role of the C-terminus is direct (e.g. by the contribution by the tail of an amino acid to the coordination complex) or indirect (e.g. by involvement in oligomerization of the antiporter) can only be confirmed by structural studies. However, these results clearly suggest that the C-terminal cytoplasmic tail does indeed play a role in antiport mediated by Vc-NhaP2.

The intriguing suggestion that the C-terminal cytoplasmic tail of Vc-NhaP2 plays a mechanistic role in antiport could represent an as-yet unobserved mechanism of antiport. At the current time, there is only a single structure available for a cation/H^+ antiporter, NhaA, which is a Na^+/H^+ antiporter. This has a C-terminal tail which consists of just 7 amino acids[66], and the structure clearly shows that none of these amino acids play a role in the mechanism of antiport of NhaA. Therefore, if our results are correct, solving the structure of Vc-NhaP2 will be of key importance to understanding the role of the C-terminal tail in NhaP2 antiport activity.

4.4. RECONSTITUTION OF ANTIPORT ACTIVITY IN THE TRUNCATION MUTANT

As is shown in Figure 7, addition of exogenous C-terminal tail to vesicles expressing the Vc-NhaP2Body significantly restored antiport activity. These results show clearly that, first, the C-terminal tail isolated by the procedure outlined above is properly folded and in its functional form. Second, it shows, in accordance with the results presented above, that the Vc-NhaP2 C-terminal tail is involved in antiport.

As discussed above, even unstructured prokaryotic C-terminal tails are capable of affecting pH specificity[67]. Therefore, it seems that while the C-terminal tail of Vc-NhaP2 is involved mechanistically in antiport in some way, the predicted domain architecture, if present, is likely needed for processes other than antiport.

4.5. CD SPECTRUM OF THE C-TERMINAL TAIL

Misfolded, disordered, or randomly coiled proteins are easily recognizable on a CD spectrum, and are characterized by very weakly negative or even positive molar absorbance difference. However, Figure 18 clearly shows the presence of 2 clear minima at 208 nm and 222 nm, which are indicative of α-helical secondary structure. Coupled with the ability of the purified Vc-NhaP2 tail to restore activity to the Vc-NhaP2Body, we can be confident that the purified protein is not random coil. The presence of secondary structural elements in the C-terminal tail verifies the predicted structure in the tail from bioinformatics approaches, which sets Vc-NhaP2 apart from all other known prokaryotic antiporters, which lack any secondary structure in their C-terminal tail domains.

4.6. DYNAMIC MULTIMERIZATION OF THE C-TERMINAL TAIL

Size-exclusion chromatography indicates that the protein is in a stable conformational state which is consistent with a monomer, whereas the DLS measurements indicate that the C-terminal tail exists in a dynamic equilibrium between a monomeric and a multimeric form. Many transmembrane ion transporters are well known to only function in dimeric[68,69,70] or higher oligomeric forms, such as tetramers[71].

The mechanism of this multimerization, however, is typically through interactions of transmembrane helices[72]. The fact that the C-terminal tail of Vc-NhaP2 clearly affects antiport, and that the C-terminal tail exhibits dynamic dimerization in solution hints that the mode by which the C-terminal tail affects antiport may be through modulation of multimeric state. Further studies will be needed to confirm whether an *in situ* role of the C-terminal tail is to regulate oligomeric state of Vc-NhaP2. However, this possibility further contributes to the collection of roles that the C-terminal tail may play in the unique Vc-NhaP2 system.

4.7. EFFECT OF FAD ON DYNAMIC MULTIMERIZATION

As discussed above, the C-terminal tail of Vc-NhaP2 is predicted to contain a TrkA-C domain which, in turn, is predicted to contain a Rossman fold. Rossman folds are known to bind dinucleotide cofactors such as NAD and FAD, and are often capable of inducing conformational changes in the protein upon binding or modification of the cofactor[73].

Unlike the initial DLS experiments in which the pH and ionic strength were varied in an attempt to stabilize the dynamic between the monomeric and multimeric states, the addition of FAD clearly has an effect on the dynamic multimerization of the Vc-NhaP2 C-terminal tail. At pH 7.0, addition of FAD to the experimental buffer stabilizes the protein in a form whose hydrodynamic radius is ~ 3 nm (Figures 12 and 17).

These results indicate that FAD stabilizes the C-terminal tail in an oligomeric state that is most probably a dimer based upon reported hydrodynamic radii for proteins of similar size from the literature[74,75]. This, however, assumes that the C-terminal tail is

globular. If it is not, there is no reason to exclude the possibility that the form observed upon FAD stabilization is a monomer.

Logically, this effect implies that FAD interacts with the protein, and is suggestive that the predicted Rossman fold from the bioinformatics analysis does, in fact, exist. If true, this makes Vc-NhaP2 a truly unique antiporter, since no cation/H^+ antiporter investigated to date interacts with a cofactor of any kind.

5. Summary and future directions

The work reported here clearly shows that the cytoplasmic tail of Vc-NhaP2 plays a significant role in both antiport efficiency and substrate affinity. This was shown both by the analyses of the Vc-NhaP2 truncation mutant and the reconstitution experiments using purified C-terminal tail. This indicates that the C-terminal tail is mechanistically involved in the antiport process, either directly or indirectly. Furthermore, DLS experiments are supportive of the idea that the predicted domain architecture for the C-terminal tail does, in fact, exist.

Purification of the C-terminal cytoplasmic tail has been achieved to 20 mg/L of culture. The purified protein has been further characterized by DLS and CD, and was of sufficient quality to perform preliminary crystallization trials. The DLS experiment indicate that the C-terminal tail exhibits a dynamic multimerization in solution which is influenced by the cofactor FAD. Future cross-linking and mutagenesis experiments could be performed to determine if an *in situ* role of the C-terminal tail is indeed to facilitate the oligomerization of the antiporter.

In addition, the predicted domain architecture in the C-terminal tail could make Vc-NhaP2 an important regulatory component in cellular metabolism. The potential roles Vc-NhaP2 could play, and their potential impact means that solving the X-ray structure of the Vc-NhaP2 C-terminal tail will be an important first step towards understanding how this K^+/H^+ antiporter functions.

Finally, given *V. cholerae*'s important status as a human pathogen, the essential role Vc-NhaP2 plays in the pathogenic cycle of *V. cholerae* makes this protein a key target for structure-based drug design. Drugs that effectively shut down Vc-NhaP2 could

prove to be valuable in the fight to control *V. cholera* outbreaks that kill thousands every year.

6. References

[1] Epstein, W. (2003) The roles and regulation of potassium in bacteria. *Prog. Nucleic Acid Res. 75.,* 293-320.

[2] Casutt, MD., Nedielkov, R., Wendelspiess, S., Vossler, S., Gerken, U., Murai, M., Miyoshi, H., Möller, HM., Steuber, J. (2011) Localization of ubiquinone-8 in the Na^+-pumping NADH:quinone oxidoreductase from *Vibrio cholerae. J. Biol. Chem. 286* (46), 40075-82.

[3] Zhu, S., Homma, M., Kojima, S. (2012) Intragenic supressor of a plug deletion nonmotility mutation in PotB, a chimeric stator protein of sodium-driven flagella. *J Bacteriol. 194* (24), 6728-35.

[4] Häse, CC., Mekalanos, JJ. (1999) Effects of changes in membrane sodium flux on virulence gene expression in *Vibrio cholerae*. *Proc. Natl. Acad. Sci. U.S.A. 96* (6), 3183-3187.

[5] Goswami, P., Paulino, C., Hizlan, D., Vonck, J., Yildiz, O., Kühlbrandt, W. (2011) Structure of the archaeal Na^+/H^+ antiporter NhaP1 and functional role of transmembrane helix 1. *EMBO J. 30* (2), 439-49.

[6] Epstein, W. (2003) The roles and regulation of potassium in bacteria. *Prog. Nucleic Acid Res. 75.,* 293-320.

[7] Zhu, S., Homma, M., Kojima, S. (2012) Intragenic supressor of a plug deletion nonmotility mutation in PotB, a chimeric stator protein of sodium-driven flagella. *J Bacteriol. 194* (24), 6728-35.

[8] Verkhovsky, MI., Bogachev, AV. (2010) Sodium-translocating NADH:quinone oxidoreductase as a redox-driven ion pump. *Biochim Biophys Acta. 1797* (6-7), 738-46.

[9] Müller, V., Aufurt, S., Rahlfs, S. (2001) The Na^+ cycle in Acetobacterium woodii: identification and characterization of a Na^+ translocation F(1)F(0)-ATPase with a mixed oligomer of 8 and 16 kDa proteolipids. *Biochim Biophys Acta. 1505* (1), 108-20.

[10] Bieber, EJ., Wilkinson, BJ. (1984). Sodium-dependent uptake or taurine in encapsulated Staphylococcus aureus strain M. *Biochim Biophys Acta. 770* (2), 127-35.

[11] Jahreis, K., Pimentel-Schmitt, EF., Brückner, R., Titgemeyer, F. (2008) Ins and outs of glucose transport systems in eubacteria. *FEMS Microbiol Rev. 32,* 891-807.

[12] Jung, H., Pirch, T., Hilger, D. (2006) Secondary transport of amino acids in prokaryotes. *J. Membrane Biol. 213*, 119-133.

[13] Li, N., Kojima, S., Homma, M. (2011) Sodium-driven motor of the polar flagellum in marine bacteria Vibrio. *Genes Cells. 16* (10), 985-99.

[14] Häse, CC., Mekalanos, JJ. (1999) Effects of changes in membrane sodium flux on virulence gene expression in *Vibrio cholerae*. *Proc. Natl. Acad. Sci. U.S.A. 96* (6), 3183-3187.

[15] Häse, CC., Fedorova, ND., Galperin, MY., Dibrov, PA. (2001) Sodium ion cycle in bacterial pathogens: evidence from cross-genome comparisons. *Microbiol. Mol. Bio. Rev. 65* (3), 353-370.

[16] Ibid.

[17] Häse, CC., Mekalanos, JJ. (1999) Effects of changes in membrane sodium flux on virulence gene expression in *Vibrio cholerae*. *Proc. Natl. Acad. Sci. U.S.A. 96* (6), 3183-3187.

[18] Häse, CC., Fedorova, ND., Galperin, MY., Dibrov, PA. (2001) Sodium ion cycle in bacterial pathogens: evidence from cross-genome comparisons. *Microbiol. Mol. Bio. Rev. 65* (3), 353-370.

[19] Resch, CT., Winogrodzki, JL., Patterson, CT., Lind, EJ., Quinn, MJ., Dibrov, P., Häse, CC. (2010) The Putative Na^+/H^+ Antiporter of *Vibrio cholerae*, Vc-NhaP2, Mediates the specific K^+/H^+ Exchange in Vivo. *Biochemistry. 49,* 2520-2528.

[20] Ibid.

[21] Ibid.

[22] Ibid.

[23] Ibid.

[24] Ibid.

[25] Hunte, C., Screpanti, E., Venturi, M., Rimon, A., Padan, E., Michel, H. (2005) Structure of a Na^+/H^+ antiporter and insights into mechanism of action and regulation by pH. *Nature. 435* (30), 1197-1202.

[26] Pinner, E., Padan, E., Schuldiner, S. (1994) Kinetic properties of NhaB, a Na^+/H^+ antiporter from Escherichia coli. *J. Biol Chem. 269,* (42), 26274-9.

[27] Dzioba, J., Ostroumov, E., Winogrodzki, A., Dibrov, P. (2002) Cloning, functional expression in Escherichia coli and primary characterization of a new Na^+/H^+ antiporter, NhaD, of Vibrio cholerae. *Mol Cell Biochem. 229,* (1-2), 119-24.

[28] Padan, E., Schuldiner, S. (1994) Molecular physiology of the Na^+/H^+ antiporter in *Escherichia coli. J. exp. Biol. 196,* 443-456.

[29] Resch, CT., Winogrodzki, JL., Häse, CC., Dibrov, P. (2011) Insights into the biochemistry of the ubiquitous NhaP family of cation/H^+ antiporters. *Biochem. Cell Bio. 89,* 130-137.

[30] Ibid.

[31] Stetefeld, J., Orriss, G. Unpublished observations.

[32] Nanatani, K., Fujiki, T., Kanou, K., Takeda-Shitaka, M., Umeyama, H., Ye, Liwen., Wang, X., Nakajima, T., Uchida, T., Maloney, P., Abe, K. (2007) Topology of AspT, the Aspartate:Alanine Anitiporter of *Tetragenococcus halophilus*, Determined by Site-Directed Fluorescence Labeling. *J. Bacteriol. 189,* (19), 7089-97.

[33] Anantharaman, V., Koonin, EV., Aravind, L. (2001) Regulatory potential, phyletic distribution and evolution of ancient, intracellular small-molecule-binding domains. *J. Mol Bio. 307,* (5), 1271-92.

[34] Ibid.

[35] Kleiger, G., Eisenberg, D. (2002) GXXG and GXXA motifs stabilize FAD and NAD(P)-binding Rossman folds through C(alpha)-H... O hydrogen bonds and van der Waals interactions. *J. Mol Bio. 323* (1), 69-76.

[36] Mewies, M., McIntire, WS., Scrutton, NS. (1998) Covalent attachment of flavin adenine dinucleotide (FAD) and flavin mononucleotide (FMN) to enzymes: the current state of affairs. *Protein Sci. 7* (1), 7-20.

[37] Iyanage, T., Xia, C., Kim, JJ. (2012) NADPH-cytochroms P450 oxidoreductase: prototypic member of the diflavin reductase family. *Arch Biochem Biophys. 528* (1), 72-89.

[38] Nelson, DL., Cox, MM. (2008) *Lehninger Principles of Biochemistry (5th ed.)*. W.H. Freeman and Company, New York. p. 520.

[39] Ibid.

[40] Dibrov, P., Fliegel, L. (1998) Comparative molecular analysis of Na^+/H^+ exchangers: a unifed model for Na^+/H^+ antiport? *FEBS Letters. 424,* (1-2), 1-5.

[41] Ibid.

[42] Slepkov, E., Fliegel, L. (2002) Structure and function of the NHE1 isoform of the Na^+/H^+ exchanger. *Biochem. Cell. Biol. 80,* 499-508.

[43] Ibid.

[44] Stetefeld, J. Unpublished observations.

[45] Slepkov, E., Fliegel, L. (2002) Structure and function of the NHE1 isoform of the Na^+/H^+ exchanger. *Biochem. Cell. Biol. 80,* 499-508.

[46] Waditee, R., Buaboocha, T., Kato, M., Hibino, T., Suzuki, S., Nakamura, T., Takabe, T. (2006) Carboxyl-terminal hydrophilic tail of a NhaP type Na+/H+ antiporter from cyanobacteria is involved in the apparent affinity for Na+ and pH sensitivity. *Arch Biochem Biophys, 450* (1), 113-21.

[47] WHO. (2010) Cholera vaccines: WHO position paper. *Weekly Epidemiological Report. 85* (13), 117-28.

[48] Sack, DA., Sack, RB., Nair, GB., Siddique, AK. (2004) Cholera. *Lancet. 363* (9404), 223-33.

[49] Ibid.

[50] Sack, DA,. Sack, RB., Chaignat, CL. (2006) Getting serious about cholera. *N. Engl. J. Med. 355* (7), 649-51.

[51] Krishna, BV., Patil, AB., Chandresekhar, MR. (2006) Fluoroquinolone-resistant *Vibrio cholerae* isolated during a cholera outbreak in India. *Trans. R. Soc. Trop. Med. Hyg. 100* (2), 224-6.

[52] Ramamurthy, T. (2008) "Antibiotic resistance in *Vibrio cholerae". Vibrio cholerae: genomics and molecular biology.* Caister Academic Press.

[53] Ohyama, T., Igarashi, K., Kobayashi, H. (1994) Physiological role of *chaA* gene in sodium and calcium circulations at high pH in *Escherichia coli. J. Bacteriol. 176*, 4311-4315.

[54] Padan, E., Maisler, N., Taglicht, D., Karpel, R., Schuldiner, S. (1989) Deletion of *ant* in *Escherichia coli* reveals its function in adaptation to high salinity and an alternative Na^+/H^+ antiporter system(s). *J. Biol. Chem. 264,* 20297-20302.

[55] Resch, CT., Winogrodzki, JL., Patterson, CT., Lind, EJ., Quinn, MJ., Dibrov, P., Häse, CC. (2010) The Putative Na^+/H^+ Antiporter of *Vibrio cholerae*, Vc-NhaP2, Mediates the specific K^+/H^+ Exchange in Vivo. *Biochemistry. 49,* 2520-2528.

[56] Dzioba-Winogrodzki, J., Winogrodzki, O., Krulwich, T.A., Boin, M.A., Häse, C.C., Dibrov, P. (2009) Characterization of the *Vibrio cholerae* multifunctional *mrp*-encoded cation/proton antiporter conferring resistance to bile salts in a heterologous host. *J. Mol. Microbiol. Biotechnol. 16,* 176-186.

[57] Patel, TR., Reuten, R., Xiong, S., Meier, M., Winzor, DJ., Koch, M., Stetefeld, J. (2012) Determination of a molecular shape for netrin-4 from hydrodynamic and small angle X-ray scattering measurements. *Matrix Biology. 31* (2), 135-140.

[58] Ohyama, T., Igarashi, K., Kobayashi, H. (1994) Physiological role of *chaA* gene in sodium and calcium circulations at high pH in *Escherichia coli*. *J. Bacteriol., 176,* 4311-4315

[59] Resch, CT., Winogrodzki, JL., Patterson, CT., Lind, EJ., Quinn, MJ., Dibrov, P., Häse, CC. (2010) The Putative Na^+/H^+ Antiporter of *Vibrio cholerae*, Vc-NhaP2, Mediates the specific K^+/H^+ Exchange in Vivo. *Biochemistry. 49,* 2520-2528.

[60] Galili, L., Rothman, K., Kozachov, L., Rimon, A., Padan, E. (2002) Transmembrane domain IV is involved in ion transport activity and pH regulation of the NhaA Na^+/H^+ antiporter of *Escherichia coli Biochemistry 41,* 609-17.

[61] Habibian, R., Dzioba, J., Barret, J., Galperin, M.Y., Loewen, P.C., Dibrov, P. (2005) Functional analysis of conserved polar residues in Vc-NhaD, Na^+/H^+ antiporter of *Vibrio cholerae. J. Biol. Chem, 280,* 39637-49.

[62] Padan, E., Tzubery, T., Herz, K., Kozachkov, L., Rimon, A., Galilii, L. (2004) NhaA of *Escherichia coli*, as a model of a pH-regulated Na^+/H^+ antiporter. *Biochim. Biophys. Acta. 1658,* 2-13.

[63] Resch, CT., Winogrodzki, JL., Patterson, CT., Lind, EJ., Quinn, MJ., Dibrov, P., Häse, CC. (2010) The Putative Na^+/H^+ Antiporter of *Vibrio cholerae*, Vc-NhaP2, Mediates the specific K^+/H^+ Exchange in Vivo. *Biochemistry. 49,* 2520-2528.

[64] Dzioba-Winogrodzki, J., Winogrodzki, O., Krulwich, T.A., Boin, M.A., Häse, C.C., Dibrov, P. (2009) Characterization of the *Vibrio cholerae* multifunctional *mrp*-encoded cation/proton antiporter conferring resistance to bile salts in a heterologous host. *J. Mol. Microbiol. Biotechnol. 16,* 176-186.

[65] Price, R., Dodds, PF. (1989). Improved Determination of K_M and V_{max} Using Weighted Linear Regression and Direct Fitting to the Michaelis-Menten Curve. *Biochemical Education. 17* (3), 138-40.

[66] Hunte, C., Screpanti, E., Venturi, M., Rimon, A., Padan, E., Michel, H. (2005) Structure of a Na^+/H^+ antiporter and insights into mechanism of action and regulation by pH. *Nature. 435* (30), 1197-1202.

[67] Waditee, R., Buaboocha, T., Kato, M., Hibino, T., Suzuki, S., Nakamura, T., Takabe, T. (2006) Carboxyl-terminal hydrophilic tail of a NhaP type Na+/H+ antiporter from cyanobacteria is involved in the apparent affinity for Na+ and pH sensitivity. *Arch Biochem Biophys, 450* (1), 113-21.

[68] Ibid.

[69] Goswami, P., Paulino, C., Hizlan, D., Vonck, J., Yidiz, O., Kühlbrandt, W. (2011) Structure of the archael Na^+/H^+ antiporter NhaP1 and functional role of transmembrane helix 1. *EMBO J. 30,* (2), 439-49.

[70] Ridilla, M., Narayanan, A., Bolin, JT., Yernool, DA. (2012) Identification of the dimer interface of a bacterial Ca^{2+}/H^+ antiporter. *Biochemistry. 51,* (48), 9603-11.

[71] Kamnesky, G., Shaked, H., Chill, JH. (2012) The distal C-terminal region of the KcsA potassium channel is a pH-dependent tetramerization domain. *J Mol Biol. 418,* (3-4), 237-47.

[72] Hunte, C., Screpanti, E., Venturi, M., Rimon, A., Padan, E., Michel, H. (2005) Structure of a Na^+/H^+ antiporter and insights into mechanism of action and regulation by pH. *Nature. 435* (30), 1197-1202.

[73] Iyanage, T., Xia, C., Kim, JJ. (2012) NADPH-cytochroms P450 oxidoreductase: prototypic member of the diflavin reductase family. *Arch Biochem Biophys. 528* (1), 72-89.

[74] Erickson, HP. (2009) Size and Shape of Protein Molecules at the Nanometer Level Determined by Sedimentation, Gel Filtration, and Electron Microscopy. *Biol Proced Online. 11,* 32-51.

[75] Armstrong, JK., Wenby, RB., Meiselman, HJ., Fisher, TC. (2004) The Hydrodynamic Radii of Macromolecules and Their Effect of Red Blood Cell Aggregation. *Biophys J. 87* (6), 4259-70.